2014

SINGLE-MOLECULE ANALYSIS OF ALZHEIMER'S β-PEPTIDE OLIGOMER DISASSEMBLY AT PHYSIOLOGICAL CONCENTRATION

Chen Chen
University of Kentucky, chenchen8899@gmail.com

STUDENT AGREEMENT:

I represent that my thesis or dissertation and abstract are my original work. Proper attribution has been given to all outside sources. I understand that I am solely responsible for obtaining any needed copyright permissions. I have obtained needed written permission statement(s) from the owner(s) of each third-party copyrighted matter to be included in my work, allowing electronic distribution (if such use is not permitted by the fair use doctrine) which will be submitted to UKnowledge as Additional File.

I hereby grant to The University of Kentucky and its agents the irrevocable, non-exclusive, and royalty-free license to archive and make accessible my work in whole or in part in all forms of media, now or hereafter known. I agree that the document mentioned above may be made available immediately for worldwide access unless an embargo applies.

I retain all other ownership rights to the copyright of my work. I also retain the right to use in future works (such as articles or books) all or part of my work. I understand that I am free to register the copyright to my work.

REVIEW, APPROVAL AND ACCEPTANCE

The document mentioned above has been reviewed and accepted by the student's advisor, on behalf of the advisory committee, and by the Director of Graduate Studies (DGS), on behalf of the program; we verify that this is the final, approved version of the student's thesis including all changes required by the advisory committee. The undersigned agree to abide by the statements above.

Chen Chen, Student

Dr. Jason DeRouchey, Major Professor

Dr. Dong-Sheng Yang, Director of Graduate Studies

SINGLE-MOLECULE ANALYSIS OF ALZHEIMER'S β-PEPTIDE OLIGOMER DISASSEMBLY AT PHYSIOLOGICAL CONCENTRATION

THESIS

A thesis submitted in partial fulfillment of the requirements
for the degree of Master of Science in the College of Arts and Sciences
at the University of Kentucky

By

Chen Chen

Lexington, Kentucky

Director: Dr. Jason DeRouchey,
Assistant Professor of Department of Chemistry

Lexington, Kentucky
2014

ABSTRACT OF THESIS

SINGLE-MOLECULE ANALYSIS OF ALZHEIMER'S β-PEPTIDE OLIGOMER DISASSEMBLY AT PHYSIOLOGICAL CONCENTRATION

The diffusible soluble oligomeric amyloid β-peptide (Aβ) has been identified as a toxic agent in Alzheimer's disease that can cause synaptic dysfunction and memory loss, indicating its role as potential therapeutic targets for AD treatment. Recently an oligomer-specific sandwich biotin-avidin interaction based assay identified the Aβ oligomer dissociation potency of a series of dihydroxybenzoic acid (DHBA) isomers. Because the sandwich assay is an ensemble method providing limited size information, fluorescence correlation spectroscopy (FCS) was employed to provide single molecule resolution of the disassembly mechanism.

Using FCS coupled with atomic force microscopy, we investigated the size distribution of fluorescein labeled synthetic Aβ oligomers at physiological concentrations, and monitored in real time the change of size and mole fraction of oligomers in the presence of dissociating agents or conditions. The higher-order dissociation process caused by DHBA isomers produced no transient oligomeric intermediates, a desirable feature for an anti-oligomer therapeutic. Urea and guanidine hydrochloride, in contrast, produced a linear dissociation with a progressive decrease of size and mole fraction of oligomers. FCS allows the facile distinction of small molecule Aβ oligomer dissociators that do not produce stable potentially toxic oligomeric Aβ intermediates.

KEYWORDS: Alzheimer's disease, soluble amyloid-β oligomers, Aβ, oligomer dissociators, fluorescence correlation spectroscopy, atomic force microscopy, dissociation mechanism

Chen Chen

03/17/2014

SINGLE-MOLECULE ANALYSIS OF ALZHEIMER'S β-PEPTIDE OLIGOMER DISASSEMBLY AT PHYSIOLOGICAL CONCENTRATION

By

Chen Chen

Jason DeRouchey, PhD
Director of Thesis

Dong-Sheng Yang, PhD
Director of Graduate Studies

03/17/2014

TABLE OF CONTENTS

LIST OF TABLES

LIST OF FIGURES

Chapter One: Introduction

1.1 Alzheimer's disease and "amyloid cascade hypothesis"

1.1.1 Overview of Alzheimer's disease

Alzheimer's disease (AD) is the most common form of dementia in many people, over the age of 65 [1]. As the most prevalent neurodegenerative disease [2], AD is clinically characterized by a progressive decline of cognitive function in multiple brain functions such as memory, thought, and behavior [3] in addition to interfering with the individuals' activities of daily life living. AD therefore imposes an enormous economic burden on society [4] and has become a serious social problem. According to recent estimates by Alzheimer's Disease International, in 2010 as many as 36 million people worldwide have AD at a resulting global cost of $604 billion [5].

There are two pathological hallmarks which are essential for a diagnosis of AD, extracellularly deposited amyloid plaques composed of amyloid-β (Aβ) peptide, 39-43 amino acids in the brain parenchyma, and intracellular neurofibrillary tangles of aggregates of hyperphosphorylated tau protein [6].

1.1.2 Genesis of the "amyloid cascade hypothesis"

.

Amyloid plaques were first described as a disease feature by the Bavarian psychiatrist Alois Alzheimer in 1906 [7], after his histological examination of the brain from his patients with AD. In 1984 Glenner and Wong isolated and identified a unique 4200 dalton protein from cerebrovascular amyloid fibril deposit in AD brain they named amyloid β-protein. They proposed that it might be derived from a unique serum precursor, which would lead to a

specific diagnosis for AD [8]. The protein comprising the hallmark neurofibrillary tangles was identified in the two years later. Hyperphosphorylated microtubule-associated tau protein was found in the paired helical filaments (PHF) inside neurons in AD. The role of tau pathology in AD became another interesting topic.

Aβ-containing amyloid plaques and neurofibrillary tangles (NFTs) were also found in the brains of the middle-aged patients with Down syndrome (DS). Thus, it was hypothesized by Glenner with his discovery of Aβ in cerebrovascular amyloid deposits from young patients with DS, that the gene encoding the amyloid precursor protein (APP), might be a causative gene for AD [9]. He postulated that the causative gene for AD was localized on the Down trisomic chromosome 21. This was confirmed subsequently by the work of Beyreuther's group [10].

The amyloid cascade hypothesis received major support in 1990 by the discovery of AD-causing mutation in a Dutch family with hereditary cerebral hemorrhage with amyloidosis, an autosomal dominant form of Aβ amyloidosis. A cytosine-to-guanine transversion mutation at amino acid 22 of the amyloid protein resulting in the change E22Q was detected and considered to initiate the deposition of the amyloid protein in the cerebrovasculature, which is similar to Aβ in AD and DS. One year later a cytosine-thymine missense mutation which caused a valine to isoleucine change at amino acid 717 in APP was found in a family with early-onset AD [11], along with subsequently identified mutations, this was taken to indicate that Aβ deposition is the central event in the pathogenesis of AD. These findings eventually led to the proposal of the "amyloid cascade hypothesis".

1.1.3 Classical "amyloid cascade hypothesis"

The amyloid cascade hypothesis (Figure 1.1), proposed by John Hardy in 1992, states that the aggregation and deposition of Aβ peptide initiates a process resulting in the human

neurodegeneration of AD [12]. Familial early onset forms of AD have been described as resulting from mutations in three different genes: the amyloid precursor protein (APP), presenilin-1 (PS1) and presenilin-2 (PS2). PS1 and PS2 are both homologous proteins that can provide the catalytic active site of γ-secretase.

The majority of type I transmembrane protein APP is processed by α-secretase, releasing the APPα ectodomain and a C-terminal fragment CTFα of 83 amino acids. CTFα is further cleaved by γ-secretase to liberate a non-toxic 23-26 amino acid p3 peptide as well as the APP intracellular domain (AICD). About 10% of APP is processed by the β-site APP cleaving enzyme (BACE) or so called β-secretase, releasing a large ectodomain of APPβ. The remaining membrane C-terminal fragment, CTFβ, containing 99 amino acids, is subsequently cleaved within the lipid bilayer by γ-secretase (presenilins 1 and 2), to produce amyloid β-protein (Aβ) and AICD. Aβ peptide spontaneously aggregates into fibrils containing cross β-sheet structure and deposits in senile plaques in the brain parenchyma or in blood vessel walls. Those fibrils and plaques can induce synaptic dysfunction and neuronal toxicity directly or indirectly by inducing cellular changes that result in the formation of the intracellular neurofibrillary tangles (NFTs) consisting of paired helical filaments (PHFs) from hyperphosphorylated tau protein, eventually resulting in AD and dementia [13].

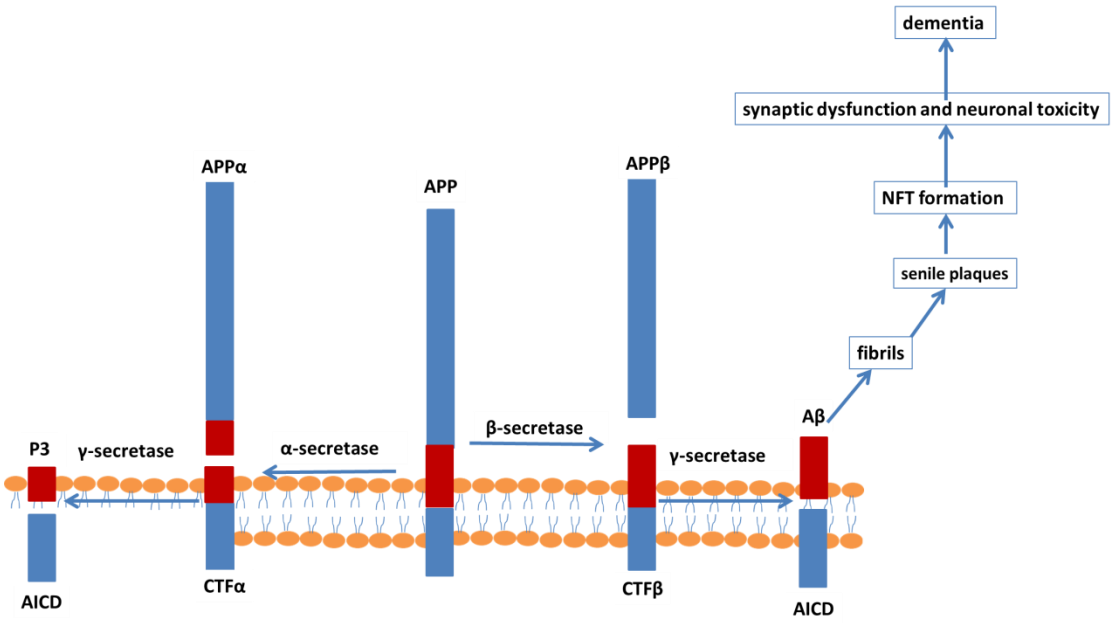

Figure 1.1. Classical "amyloid cascade hypothesis"

1.1.4 Misfolded Aβ assembly pathway: oligomers and fibrils

The secretase-cleaved Aβ peptides with 39-42 amino acid residues are released from the cell and can convert from random coil to cross β strand or α-helix in the formation of Aβ fibrils [14]. Even though Aβ monomers are relative harmless, and may serve some positive biological function, they can also self-assemble via a nucleation-dependent pathway (Figure 1.2) into soluble Aβ oligomers, larger Aβ aggregation intermediates, protofibrils, and eventually the fibrillar aggregates that deposit in the brain [15].

Those soluble oligomers ranging from low molecular weight (~2-8 monomers) to high molecular weight (~20-40 monomers) species appear in the early stages of aggregation from monomers to insoluble fibrils following classical polymerization kinetics. In addition, off pathway oligomers, or called "prefibrillar oligomers" which do not directly continue on to form fibrils, have also been identified [16], indicating that there are at least two independent Aβ assembly pathways, one leading to off pathway oligomers and the other to fibrils. These two different types of oligomers, prefibrillar oligomers and fibrillar oligomers can be distinguished by conformational epitope-specific antibodies. The fibrillar specific antibody, OC, only recognizes the generic fibrillar lattice structure of fibrillar oligomers protofibrils, or mature fibrils. Another antibody, A11, only recognizes a generic epitope of prefibrillar oligomers [17]. The definition of "soluble" refers to Aβ in aqueous buffer that is not pelleted after high-speed centrifugation (100,000 xg, 1 hour) [18]. Synthetic oligomers have different sizes and structure as well as morphology resulting from different sample preparation processes. The relationship between synthetic and biological oligomers structure, stability, and biological activity is unknown and is the topic of intense debate. Due to the surfactant properties of axially amphipathic Aβ peptide, synthetic oligomers likely have a micellar structure with a hydrophobic core stabilized by the "hydrophobic effect" [19].

Fibril formation is frequently nucleated on extracellular matrix or cell surfaces. The structure of short synthetic peptide amyloid fibrils is recently described as "steric zippers" with a

cross-β spine composed of a pair of parallel hydrogen-bonded β-sheet strands [20]. The nucleation and elongation of fibril for both synthetic and AD brain deposited fibrils is proportional to the Aβ monomer concentration [21]. The synthetic fibrils are usually prepared at relatively high concentrations of peptide. Amyloid fibrils from different proteins or even growing from identical sequences can have different structural detail and conformations as polymorphisms on the basic cross-β sheet backbone as detected by relative seeding efficiencies, indicating high sensitivity to point mutations at certain positions in the Aβ and high specificity in general seeding of fibril elongation [22]. Aβ assembly pathway is thermodynamically a reversible process, and deposited fibrils could disassemble into soluble oligomers, although this is kinetically slow. A recent study suggests that large insoluble Aβ deposits might be a potential reservoir for soluble oligomers [23]. Extrapolation to biological systems, in particular to the human condition is poorly studied.

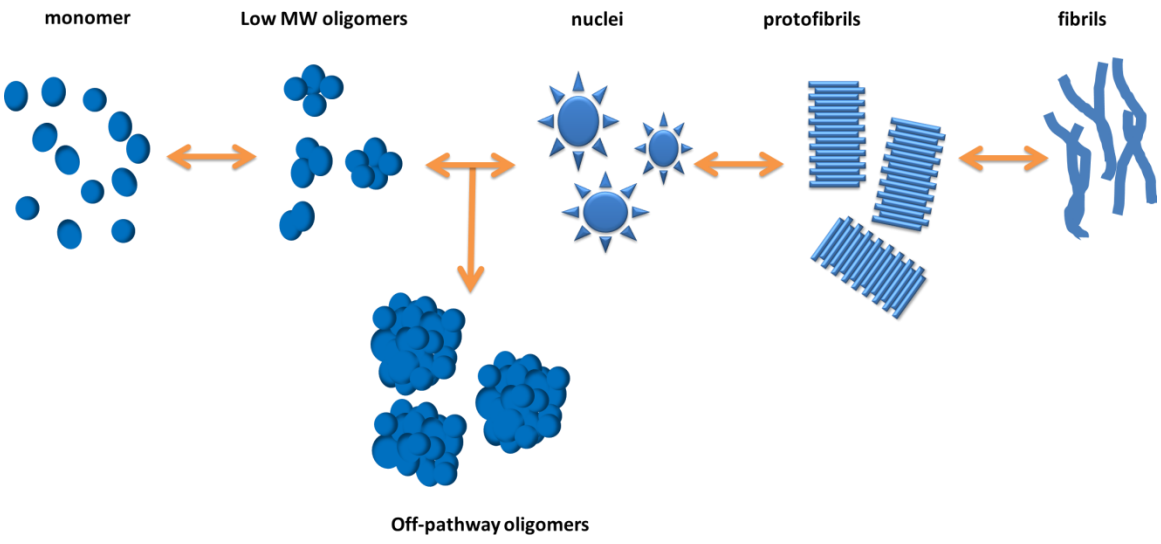

Figure 1.2. Schematic diagram of Aβ aggregation process

1.1.5 Misfolded proteins in other neurodegenerative diseases

The presence of intra- or extracellular amyloid deposits of misfolded, aggregated proteins in the brain have been identified in other neurodegenerative disease, including Parkinson's disease (PD), Huntington's disease (HD), transmissible spongiform encephalopathies (TSE), and amyotrophic lateral sclerosis (ALS, or Lou Gehrig's disease) [24]. Amyloids have traditionally been defined by their solubility, morphology and ability to bind dyes, like Congo red with birefringence and thioflavin T with a specific fluorescence change.

The protein, α-synuclein, was found as the major component of the cytopathological hallmarks in PD, Lewy bodies and Lewy neurites, observed in the cytoplasm. Natively unfolded (intrinsically disordered) in solution, α-synuclein is a soluble cytoplasmic protein that is highly expressed in neurons, containing an α-helical region, which helps bind to the phospholipid membranes of synaptic vesicles [25]. In HD, diffuse, severe atrophy of the neostriatum is the diagnosis hallmark in HD, of which the polyglutamine-rich protein huntingtin aggregates in neuronal intranuclear and cytoplasmic inclusions [26]. In TSE, or prion disease, a fundamental event is responsible for the neurotoxicity, which describes the conversion from natively folded glycoprotein PrPC to pathogenic conformation PrPSc which is protease-resistant and assembles in amyloid and other deposits [27]. The misfolding of copper–zinc superoxide dismutase (SOD 1) and conversion from soluble SOD1 to amyloid fibrils in the spinal cord is thought to be the main cause of a subset of familial and ALS [28].

Interestingly, amyloid fibrils share similar morphology and structure even though the specific composing protein for each disease has different sequences. The conformation-dependent anti-oligomer and anti-fibril antibodies recognize the oligomers and the fibrils regardless of sequence, indicating the possible existence of a common pathogenic mechanism [29].

However the mechanism by which aggregation of misfolded proteins leads to synaptic dysfunction in neurodegenerative disorders remains to be clarified. Thus, the study of the

experimentally accessible Aβ assembly-disassembly mechanism in AD could provide a general model system which could be applicable to other diseases.

1.1.6 Modified amyloid hypothesis: relation between amyloid plaques and neurofibrillary tangles

There are 2 different types of protein deposits, amyloid plaques (APs) and neurofibrillary tangles (NFTs) in AD pathology. APs are extracellular deposits of insoluble Aβ fibrils in the parenchyma and around the cerebral blood vessel walls, with 39- 42 amino acids and the main component are Aβ1-40 and Aβ1-42. In contrast, usually deposited intracellularly in the cytoplasm of degenerating neurons, NFTs are composed of paired helical filaments (PHF) formed from hyperphosphorylated tau. However, it was controversial which one occurs early in the disease process and whether they contribute equally to cognitive decline since the early description about AD has been based on the studies of AD brain at the end stage.

This was clarified by clinicopathologic studies of AP and NFT with the AD brain samples at different stages [30]. The presence of APs and NFTs in autopsy specimens from multiple cortical regions was compared, among elderly non-AD subjects (cognitively normal) and subjects with different severity of AD evaluated by their last cognitive test, a Mini-Mental State Examination, before death. Before significant cognitive deficits were observed, the significant differences were in the amounts of APs, suggesting that amyloid plaques are related to the earliest cognitive signs of AD. In later stages of pathology the severity of dementia was much more closely related to NFT burden than to Aβ deposition, even though the density of both pathologies increased with the severity of AD, suggesting that NFTs as major markers of severe cognitive impairment and dementia [31].

As a result, the “amyloid cascade hypothesis” was modified considering the role of later stage tau pathology where NFTs are present. This is supported by the finding that mutations in the

tau gene cause autosomal dominantly inherited dementia linked to chromosome 17 (FTPD-17), indicating that tau pathology is sufficient to cause neuronal loss [32]. The tau deposition occurs in different brain regions and affects different brain functional modalities than in AD. Thus, in AD, tau pathology is believed by many to act downstream of Aβ pathology [33] .

In summary, cognitive impairment in Alzheimer disease appears to be driven by amyloid plaques and neurofibrillary tangles at different stages of the disease, as described by the modified "amyloid cascade hypothesis". The aggregation and deposition of Aβ, occurs at a very early stage initiating synaptic dysfunction and triggering tau pathology. Tau pathology develops downstream of Aβ pathology, correlates tightly with neuronal loss, and eventually AD-type dementia.

1.2 Toxic soluble Aβ oligomers

1.2.1 Soluble Aβ oligomers: major toxins in AD

Since the "amyloid cascade hypothesis" was first proposed by John Hardy and David Allsop [12] nearly one decade ago, it has long been hypothesized that extracellular plaques of Aβ fibrils induce neurodegeneration in AD, as those insoluble fibrillar assemblies are found neurotoxic *in vitro* [34]. Yet recent studies show that the level of senile plaques is relatively weakly correlated with the severity of dementia or other cognitive alterations, either in human or in the mouse model of AD [35,36]. Non-demented individuals have been reported that have same amount of insoluble amyloid deposits as cognitively impaired subjects. This disparity led to further modification of the cascade hypothesis by suggesting that the primary toxic species in AD are soluble prefibrillar or fibrillar oligomeric aggregates formed in the early stage of aggregation, rather than the mature fibrils [37,38].

The classic “amyloid cascade hypothesis” has been modified over the years when it became clearer that there was a more robust correlation between the level of soluble oligomeric, rather than fibrillar Aβ and the extent of cognitive impairment, dementia, and disease severity [39]. Lambert *et al.* [40] reported that soluble synthetic Aβ1-42 oligomers, assembled in the absence of fibril formation, and named Abeta-derived diffusible ligands (ADDLs), were responsible for death of neurons in rat embryonic organotypic central nervous system cultures. Electrophysiological studies with protofibrils (PF), metastable intermediates in amyloid fibril formation, showed the ability of those earlier Aβ assemblies, especially high molecular weight species, to induce toxicity in primary neuronal cultures without any evidence of significant conversion to fibrils [41]. Furthermore, intracerebral microinjection of cell culture medium containing biological Aβ oligomers blocked long-term potentiation (LTP) in the rat hippocampus *in vivo*, a mechanism thought to be relate synaptic plasticity to both learning and memory [42]. A 56-kDa soluble oligomeric amyloid-β assembly, Aβ56*, purified from the brains of cognitively impaired Tg2576 mice, induced a similar synaptotoxic effect and disrupted memory when infused into the brain of normal rats [43]. These studies strongly support the hypothesis that non-fibrillar oligomeric forms of Aβ are potential toxic agents in AD.

1.2.2 Other toxic forms of Aβ present in AD brain

Beside the Aβ1-40 and Aβ1-42, various N- and C-terminal chemical modifications have been found through *in vitro* and *in vivo* analyses of amyloid deposits in AD [44,45,46], which also strongly influence and thus may play important roles in amyloid-β peptide aggregation and deposition.

A recent study suggested Aβ1-43, as a novel toxic peptide in AD. This longer and more hydrophobic peptide has a higher propensity to aggregate and is more neurotoxic than Aβ42 [47]. Moreover, several N-terminal truncation and modifications such as pyroglutamate

formation of Aβ have also been reported. Aβ4–42 was detected as a relatively abundant species in the Aβ1-42 fraction the predominant form of extracted Aβ present in the brain of AD and vascular dementia patients [48]. AβpE3, starting with pyroglutamate by cyclization at residue Glu-3 was reported to present in equivalent or larger amounts than full-length Aβ in senile plaques, which was confirmed by the analysis of water-soluble Aβ, indicating AβpE3-42 is the predominant Aβ species in AD and Down syndrome [49]. Portelius *et al.* showed by employment of immunoprecipitation and mass spectrometry, that Aβ1–40, Aβ1–42, AβpE3–42, and Aβ4–42 are the dominant plaque components in the brains of sporadic AD and familial AD [50]. Many studies demonstrated that N-terminal deletions and modifications can enhance Aβ aggregation, generating more toxic species than wild type Aβ. Moreover, other modifications have also been reported, for instance, aspartate isomerization and racemization, which both have been shown to enhance peptide aggregation and fibril formation [51,52]. Interestingly, these modifications are not found in significant amounts in AD animal model Aβ pathology [53]. The effect of these modifications on soluble oligomer formation *in vitro* or *in vivo* has not been established.

1.2.3 Importance to study Aβ oligomers

In conclusion, it is important to study the assembly and toxicity mechanism of Aβ oligomers because: i) compared with fibrils, oligomeric Aβ are much smaller and more soluble which can readily diffuse through the brain parenchyma and induce synaptic dysfunction and memory loss. ii) As discussed in Section 1.6, the aggregation of Aβ is the early event in AD pathologic process, and it triggers the downstream tau pathology, which is better correlated with dementia. Also, Aβ oligomers treatment of cells causes intracellular tau to misfold.[54]. iii) Biological Aβ oligomers with a high degree of heterogeneity have been described as various assembly forms with different sizes and structure, resulting in different neuronal toxicities. iv) as mentioned in Section 1.5, the misfolded protein in other neurodegenerative disease such as PD and HD also can form small oligomeric assemblies with similar amyloid

structural feature as Aβ oligomers, suggesting that they could share a common mechanism of toxicity, despite their different amino acid sequence. Therefore the study of Aβ oligomers may translate to other misfolded protein oligomers might aid in their diagnosis and therapeutic treatment.

1.3 How do oligomers impair memory?

As a classical cellular model that underlies learning and memory as well as synaptic plasticity, long-term potentiation (LTP) is under intensive study. LTP and long-term depression (LTD) are complementary cellular models of learning and memory that constitute an attractive means of detecting perturbations of synaptic functioning in the absence of overt neuronal death [55].

Reports from numerous laboratories have now documented that both synthetic soluble and naturally secreted Aβ oligomers such as ADDLs can inhibit hippocampal LTP and disrupt memory function, in the absence of amyloid fibrils. But only a few studies have examined the impact of Aβ on LTD. A detailed study demonstrates that Aβ oligomers interfere with synaptic plasticity by blocking both tetanus-induced LTP and the reversal of LTD but completely sparing low-frequency LTD in rat dentate gyrus [55].

The mechanisms of soluble Aβ oligomer formation *in vivo* and how they interact with neuronal cells leading to synaptic dysfunction and memory loss still remains unclear. The production of Aβ can depress synaptic transmission and the level of Aβ is correlated with synaptic activity *in vivo* in a transgenic mouse model [56,57]. Since an initial report of neuronal surface binding of soluble Aβ oligomers [3], subsequent observations have reported specific binding of synthetic and biological oligomers to neuronal synaptic regions in hippocampus and cerebral cortex [39,40]. Both receptor binding and membrane permeabilization mechanisms have been studied (Figure 1.3).

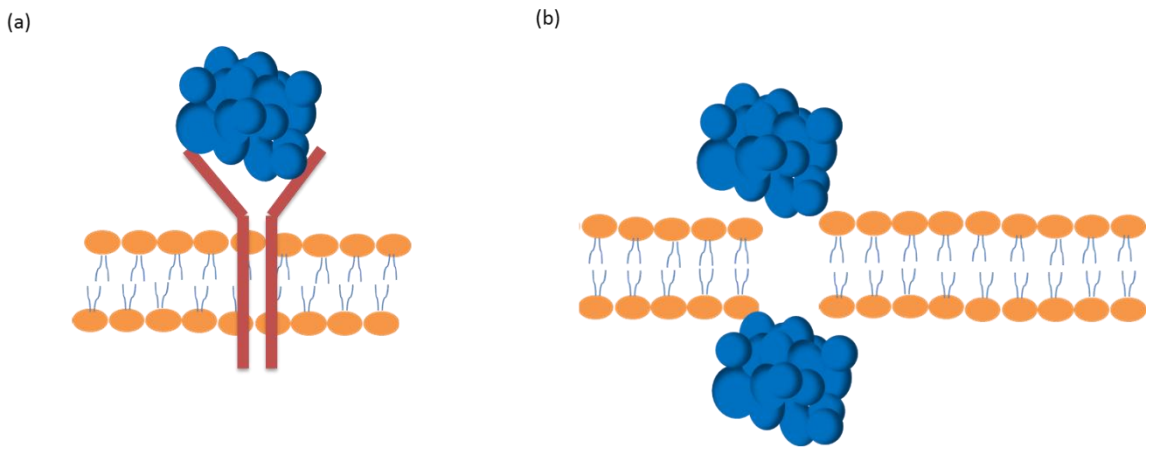

Figure 1.3. Toxicity mechanisms of soluble Aβ oligomers.
a, receptor-mediated binding; b, pore-forming permeabilization.

1.3.1 Receptor-mediated binding mechanisms

Formation of soluble Aβ oligomers *in vivo* can be induced by gangliosides such as GM1 located on the membrane [58] and extracellular soluble proteins such as αB-crystallin and ApoJ. A variety of cell membrane-associated receptors have been reported to bind soluble Aβ oligomers, including nerve growth factor receptor (NGF-R), N-methyl-d-aspartate (NMDA)-type glutamate receptor (NMDA-R), insulin receptor, Frizzled receptor, and prion protein (PrPC). The interaction between peptide and receptors requires peptide aggregation, and is not sequence specific or stereospecific [17].

Compelling evidence from Yamamoto *et al.* demonstrates that the globular Aβ oligomers are formed rapidly in the presence of GM1 gangliosides and bind with NGF receptor, triggers the activation of apoptotic signaling and induces neuronal cell death [58]. Binding of ADDLs influences signaling pathways downstream of NMDA-type glutamate receptor on synaptic plasma membranes, causing neuronal damage through NMDA-R-dependent calcium influx, resulting in neuronal oxidative stress and synapse loss [59,60]. ADDLs can interfere with insulin receptor function at the cell surface and block specific kinases required for long term potentiation (LTP) [61]. Frizzled receptor–mediated binding of ADDLs causes the inhibition

of Wnt protein signaling, which is associated with tau pathology [62]. Prion protein PrPC on the cell surface binds prefibrillar oligomers at nanomolar concentrations, leading to impairment of synaptic plasticity [63].

1.3.2 Pore-forming permeabilization mechanisms

There is another plausible mechanism for Aβ oligomer toxicity, pore-mediated permeabilization mechanisms, as proposed several years ago by Rojas and co-workers [64]. The cell membrane is destabilized by the Aβ oligomers, resulting in the formation of cation-selective membrane pores and dysregulation of ion homeostasis, such as Ca 2+ [65]. Arispe *et al.* in 1993 first reported the formation of calcium- and other cation- selective channels in bilayer membranes by Aβ oligomers [66] followed by the finding of the formation of amyloid pores on the cell surface from pathogenic mutations [67]. The mechanism of permeabilization was clarified by subsequent studies suggesting that regardless of sequence soluble amyloid oligomers increase bilayer conductance by altering the dielectric structure of the membrane, leading to a conformation-specific permeabilization of lipid bilayers [68,69]. Importantly, the conductance of lipid bilayers was not increased by fibrils or monomers, indicating that permeabilization is a specific property of amyloid oligomers related to oligomer structure.

1.4 Review of recent studies of Aβ oligomers

1.4.1 Detection and characterization of Aβ oligomers

Recent techniques employed to study soluble Aβ oligomers mostly focus on, quantitative analysis of sizes of monomer and different oligomers, and on qualitative identification and characterization of oligomers. Real-time monitoring of the size changes of oligomers is

desired during testing for assembly modulatory compounds when Aβ oligomers are the main target in therapy strategy. Understanding the structure and conformation of Aβ as well as the assembly-disassembly mechanism may provide insight into anti-AD drug design therapeutic intervention.

The early tools for diagnostic testing for amyloid fibrils in tissue, the birefringence of the histologic dye, Congo red and fluorescence of thioflavin T have been widely used to characterize Aβ assemblies in the later stages of aggregation into fibrils, but they are not applicable to the early assembly stages and suffer from low sensitivity [70,71]. A variety of other techniques have been employed in the study of aggregation of Aβ [72]. A widely used electrophoretic technique for the size analysis of Aβ oligomers is sodium dodecyl sulfate polyacrylamide gel separation (SDS -PAGE). Other techniques for studying assembly size distribution include photochemical cross-linking (PICUP) followed by SDS-PAGE, size-exclusion chromatography (SEC), analytical ultracentrifugation (AUC), dynamic light scattering (DLS), ion-mobility spectrometry–mass spectrometry (IMS–MS), and fluorescence correlation spectroscopy (FCS). Techniques including single-site enzyme-linked immunosorbent assay (ELISA) and dot blotting with oligomer-specific antibodies have been applied to detect Aβ oligomers. However, these last two methods do not provide size information.

Table 1.1. Summary and characterization of different types of oligomeric soluble Aβ

Oligomers	**Type**	**Characteristics**	**Size**	**MW**	**Reference**
soluble dimers and trimers	Natural	secreted from human brain and amyloid plaque extraction; SDS-stable; block LTP *in vitro*	1-3 nm in height and 5-10 nm in width/length	~8kDa and ~12kDa	[42], [73]
Aβ*56	Natural	SDS-stable dodecamers correlated with memory loss in APP ransgenic Tg2576 mice model	N/A	56kDa	[43]
Aβ-derived diffusible ligands (ADDLs)	Synthetic	Small soluble globular structures; bind to dendritic arbors of cultured neurons; disrupt LTP at very low concentration	5 nm in diameter	Mainly 17 and 22 kDa	[40]
annular Aβ oligomers	Synthetic	Doughnut-like structures, formed from mutant Aβ	8-12 nm(outer diameter) and 2.0-2.5 nm (inner diameter)	150–250 kDa	[74], [75]
Amylospheroid (ASPDs)	Synthetic	spheroidal structures highly neurotoxic, off-pathway,	10-15 nm in diameter	~330kDa	[76]
protofibrils (PFs)	Synthetic	Intermediates of Aβ fibril formation; β-sheet structure: bind Congo red and Thioflavin T	<150 nm in length and ~5 nm in width	>100kDa	[41], [77]

1.4.2 Kinetics studies of Aβ assembly and dissociation

The underlying kinetics of assembly and dissociation of soluble Aβ oligomers are currently not very well understood because oligomers are transient and heterogeneous, even though the nucleation-dependent polymerization model for fibril formation is generally accepted [78].

The assembly of pre-fibrillar oligomers formed during the aggregation of the SH3 domain of PI3 kinase was studied by single-molecule fluorescence two-color coincidence detection (TCCD) [79]. Fibrils are formed with the accumulation of pre-fibrillar oligomers whose stability increases with time. At the early stage of aggregation those maximally cytotoxic species are a heterogeneous ensemble of oligomers with a median size of 38±10 protein molecules per oligomer, similar to estimated critical size of small oligomeric "seed" of fibril formation in AD and PD. There is a pronounced change in stability between soluble oligomers and fibrils indicating a general mechanism of amyloid aggregation in which those oligomeric species undergo an internal conformational reorganization during nucleation phase of fibril formation. This result is in line with the process predicted by computer simulations which involves a reorganization process of oligomers driven by interchain hydrogen bonding interactions that induce nucleation of the cross-β structure [80].

Kinetic stability of Aβ oligomers was described in a recent study and the off-rate of Aβ monomers dissociating from protofibrils was determined in the presence of an engineered Aβ-binding protein ZAβ3, which blocks Aβ aggregation by selectively sequestering monomers. The dissociation of monomers from Aβ protofibrils follows monoexponential decay kinetics with a slow rate and high activation energy, which is consistent with a dissociation model of oligomers reported in the previous study with treatment of small molecular assembly inhibitors [81].

1.4.3 Single-molecule studies of Aβ oligomers

Compared with traditional ensemble techniques, single molecule techniques provide a complementary method for quantification and qualification of Aβ oligomers. Advantages of the single molecule techniques include low concentration (~nanomolar), fast real-time monitoring, and individual particle resolution regardless of sample heterogeneity.

Recently a single molecule study based on photobleaching of fluorescently labeled Aβ was developed to determine the number of monomers in an oligomer [82]. The number of monomers forming individual oligomers is equal to the number of photobleaching events from excited fluorophores present in that oligomer. Thus the size of oligomers could be determined from recorded number of photobleaching steps. By building up a histogram of the number of subunits in each photobleached oligomer, the whole oligomer size distribution was extracted and then analyzed by Monte Carlo simulations. Although this approach is only suitable for oligomers containing low numbers of monomers (such as hexamer), the result was in close agreement with the oligomer size distribution from HPLC size exclusion gel filtration. Single molecule step-wise photobleaching is a novel avenue to study the size distribution of small Aβ assembly ensembles with high heterogeneity.

As one of the advanced single molecule techniques, FCS has been widely used for detection of diffusion of fluorescence labeled Aβ monomers and oligomers in aqueous systems. By detecting the fluorescence intensity fluctuations as each single dye-labeled particle passes through a well-defined confocal volume, FCS can provide the number of fluorescent particles and diffusion time, which relate to the concentration and size of the particles, respectively. In 1998 Pitschke *et al* developed a method to study the seeded multimerization process using FCS, by adding fluorescent labeled synthetic Aβ(1-42) peptide to pre-existing aggregate "seed" in cerebrospinal fluid samples from Alzheimer's patients [83]. In contrast to cerebrospinal fluid control, only the AD-sample generated the high intensity fluorescent events from fluorescent labeled synthetic peptide bound to multimeric species suggesting that Aβ

multimers could potentially be a bio-marker for AD diagnosis. Almost at the same time Tjernberg *et al.* showed the utility of FCS for the study of the inhibition of Aβ polymerization *in vitro* by synthetic Aβ ligand LBMP1620 labeled with the fluorescent dye rhodamine [84]. The Aβ ligand could inhibit the polymerization process at early stages. In this thesis, the mechanism of Aβ assembly-disassembly will be explored by FCS at near physiological concentrations of Aβ(1-42) peptide.

1.5 Mechanism study of Aβ1-42 assembly-disassembly at near physiological concentration

1.5.1 Aβ1-42 and oligomerization

In this thesis synthetic Aβ1-42 is used to form the main target Aβ oligomers, since they are the major species composing the deposited plaque in the brain [85] and Aβ oligomerization process is more facile with Aβ1-42 than with Aβ1-40 [74].

Aβ oligomerization is closely related with enzymatic process and familial AD mutations. Since the second endoprotease, γ-secreatase in the enzymatic process cleaves at different sites which occur after amino acid 38, 40, 42. The resulting Aβs vary in length of polypeptide chain, as well as self-aggregating potential. The most biologically abundant Aβ peptide circulated in extracellular fluids like blood plasma and cerebrospinal fluid is Aβ 1-40 (80%-90%). However, Aβ1-42 (5%-10%) oligomerizes much more readily than Aβ1-40 due to its highly hydrophobic C-terminus with two additional hydrophobic amino acid residues (alanine and isoleucine).

The method of photo-induced crosslinking of unmodified proteins (PICUP) [86] has been used recently to covalently stabilize the early unstable intermediates of Aβ aggregation and to elucidate the size distribution of the early stages of Aβ1-40 and Aβ1-42 assembly, by

combining with SDS-PAGE and size exclusion chromatography (SEC). Aβ1-42 stepwise forms paranuclei (pentamer/hexamer) units that self-associate to form higher-order oligomers like early protofibrils whereas Aβ1-40, instead of paranuclei, produces a mixture of monomer, dimer, trimer, and tetramer [74]. This unique fundamental feature, paranucleus formation by Aβ1-42, provides an explanation for its strong correlation with AD.

Familial AD mutations in the N-terminal and C-terminal regions of the Aβ peptide in APP and in PS1/ PS2 elevate the ratio of Aβ1-42/Aβ1-40, which inversely correlates with age of disease onset and directly with Aβ aggregation level. One recent study demonstrated that the mean age of familial AD onset in caused by PS1 mutations correlates inversely with the Aβ1-42/Aβ1-40 ratio (either increased Aβ1-42 production or reduced Aβ1-40 level) [87]. Furthermore, enhancement of Aβ1-40 production, but not Aβ1-42 reduces the deposition of Aβ1-42 in brain in a transgenic mouse model [85].

1.5.2 Relationship of the concentration of synthetic Aβ peptide for oligomer formation in vitro to in vivo monomer concentrations

Studies on Aβ oligomers have been conducted primarily with high concentrations of synthetic Aβ peptides, mainly Aβ1-40 and Aβ1-42, as a model for Aβ assemblies found in the brains of AD patients. Aβ oligomers have been prepared at different concentrations since the type of Aβ peptide, preparation conditions, buffer ions, and incubation time can lead to different critical concentrations for oligomer formation. Surface tension measurements followed by SDS-PAGE showed that Aβ1-36 residues or longer in water has a critical concentration of ~25 μM below which only monomers and dimers are observed [19]. In the study of divalent metal ion interactions with Aβ oligomers, the oligomers were prepared by incubating a mixture of 60μM Aβ1-40 with 100 nM rhodamine-labeled Aβ1–40 in Hepes buffer for 48 hrs. The resultant size distribution analyzed by FCS included monomer and low molecular oligomers (1.2 to 3.0 nm) as well as larger oligomers (50 to 120 nm) [88]. In the PICUP

experiment in section 1.5.1 the paranuclei (pentamer/hexamer) of Aβ1-42 were formed in a 1 μM solution (in 20 mM sodium phosphate buffer, pH 7.4) [74], whereas a rapid equilibrium involving monomer, dimer, trimer, and tetramer for Aβ1-40 prior to further assembly was observed at a concentration of 20 μM [89].

However, these high concentrations are not consistent with the physiological concentrations of amyloid-β peptide, typically nanomolar to sub-nanomolar in cerebrospinal fluid and plasma, similar to the concentration of naturally secreted Aβ by cultured cells. At these low concentrations, the assembly of the peptide into oligomers differ in the kinetics of formation and possibly also in structure [90].

In our study the Aβ1-42 oligomer solutions are prepared at the tens of nanomolar concentration by the preparation method used for the sandwich ELISA study by LeVine [91] , which make it possible to study the assembly-disassembly mechanisms of oligomers at near physiological peptide concentrations. According to LeVine's study, large oligomers with molecular weight of 220 kDa and higher by size exclusion chromatography can be formed from synthetic Aβ1-42 at a concentration of 1–20nM when diluted from dimethyl sulfoxide or 1,1,1,3,3,3-hexafluoro-2-propanol. These oligomers are the same size as those observed by SEC of soluble extracts of AD brain and an AD pathology mouse model brain [7,92].

1.5.3 Oligomers as therapeutic target

The soluble Aβ oligomeric species are the principle focus of our study since they are the main toxic species in AD which cause early synaptic dysfunction and memory loss, and also trigger downstream tau pathology. Both natural and synthetic oligomers have been studied for their disassembly mechanism. Cell culture-produced biological Aβ oligomers and oligomers isolated from transgenic mice are considerably more stable to disassembly than those formed from synthetic peptide [43]. *In vitro* incubation of synthetic Aβ (1–42) peptide produces a

series of rapidly exchanging unstable low-n oligomers culminating in a proportion of relatively stable 12–24-mers that can associate to higher order species. These soluble misfolded oligomers of the Alzheimer's Aβ peptide are significantly more toxic to neurons and other cell types than are monomers or fibrils [12].

People have been attempting to target oligomers directly and indirectly in many ways. Potent highly selective inhibitors of BACE and γ-secretase that can readily enter the brain lower the production of monomers as well as oligomers. Eli Lilly and Company tested the efficacy of a functional γ-secretase inhibitor, LY450139 in phase II trials [93]. Preclinically, this compound had already been shown to reduce the rate of formation of Aβ *in vitro* and *in vivo*. While this approach is effective at reducing Aβ production, disruption of these proteases which have many other substrates besides APP has the potential to cause side effects.

Based on the discovery of a receptor-mediated toxicity mechanism, as introduced earlier, development of oligomer receptor antagonists is also a possibility. When the receptor is the target of the right type of small molecule antagonist, soluble Aβ oligomers effects could be reduced. This is likely to be complicated as effects on the interaction of the native ligand with its receptor must also be considered. Recently efforts have been made to target the neurotransmitter pathway mediated by the *N*-Methyl-D-aspartate (NMDA) receptor. Memantine, a low-moderate affinity uncompetitive NMDA receptor antagonist, has been approved by the U.S. Food and Drug Administration for treatment of moderate-to-severe AD in 2003 [94]. Interestingly, a recent study shows there is little evidence of any benefit in mild Alzheimer's disease [95].

One of the furthest advanced methods is reduction of Aβ monomer and oligomers by immunotherapy either passively with anti-Aβ antibodies or by active Aβ vaccination. Since Solomon *et al.* reported in 1996 *in vitr*o epitope-dependent inhibition of Aβ fibrillation by monoclonal antibodies [96], one effective mechanism of immunotherapy was described by McLaurin *et al.* for antibodies selective for residues 4–10 of Aβ1-42 which blocked synthetic Aβ oligomerization and cytotoxicity [97]. The *in vivo* study of peripheral injection of an

oligomer-specific antibody normalized cognitive behavior and synaptic deficits in APP transgenic AD mice, providing direct support for the use of selective Aβ oligomer-binding antibodies to improve cognition in AD patients [98]. Moreover, endogenous antibodies that were raised by active Aβ vaccination also had the ability to neutralize oligomers and prevent the inhibition of LTP *in vivo* [99]. However, immunization also interferes with production of monomers which are thought to have a positive, modulatory effect on synaptic plasticity and memory in low concentrations [100]. Moreover, dosing in a phase II clinical immunization trial of AN-1792 Aβ vaccine was suspended when an encephalitis side effect was found in a subset of patients. There were no measureable effects on cognition even though much of the insoluble Aβ pathology was cleared [101]. The encephalitis side effect of the AN-1792 immunization procedure has since been corrected and additional immunization trials are underway.

An alternative directly therapeutic approach is blocking the assembly of soluble Aβ oligomers from monomer or dissociating the preformed oligomers. A number of drug discovery efforts involving high throughput screening of small-molecule libraries have led to the discovery of efficacious assembly inhibitors. The inhibitory effects of clioquinol and other 8-hydroxyquinoline derivatives on Aβ assembly *in vitro* were identified with a single-site biotinylated Aβ1–42 oligomer assembly assay from the screening of the NINDS-Custom Collection of 1040 drugs and biologically active compounds [102]. Interestingly, the inhibition activity is not related to their chelating activity, even though clioquinol can chelate zinc and copper and inhibit aggregation caused by these metal ions. Prana Biotechnology is pursing therapeutic applications of this class of molecules.

1. 5.4 Dissociation of oligomers with DHBA isomers and other compounds

Dissociation of preformed oligomers by potent small molecules is a less often pursued therapeutic avenue as most literature assays are not configured to monitor this process. In our

study, a series of dihydroxybenzoic acid (DHBA) isomers as well as other dissociating compounds are used to study the disassembly mechanism of soluble Aβ(1-42) peptide oligomers. They were discovered using a dissociator screen of a small molecule structural diversity compound library [103]. Studies of the DHBA isomers with a biotin-avidin interaction-based ELISA assay coupled with size exclusion chromatography and PICUP, showed that the DHBA isomers have no effect on assembly, but a hydroxyl position-dependent ability to dissociate preformed oligomers. A model of the dissociation process was posited that these compounds progressively dissociate monomers from oligomers rather than fissioning oligomers into smaller intermediates, since intermediate size species were observed. However, the model is not very well defined because the oligomer detection method employed does not provide size determination. The single-site assay cannot distinguish large numbers of small oligomers from small numbers of relative larger oligomers if both of them have an identical number of exposed biotins. Oligomers with molecular weight below than 40-50 kDa are poorly detected by the single-site assay. In addition, large aggregates also might not be detected quantitatively since it is possible that a significant number of biotins are inaccessible due to oligomer shapes [104]. Therefore, a single-molecule detection method becomes a necessary tool here in order to provide an accurate quantification of numbers of oligomers of different sizes in a heterogeneous population.

In this study, by using fluorescence correlation spectroscopy coupled with atomic force spectroscopy, we were able to not only measure the size distribution of amyloid-β oligomer sample over a wide range of sizes at physiological concentrations (~nM), but also to monitor the change of size and fraction of oligomers during the dissociation process in real time.

Chapter Two: Materials and Methods

2.1 Experimental

2.1.1 Chemicals and products

The benzoic acid derivatives, Tween 20 (ultrapure), 1,1,1,3,3,3-hexafluoro-2-propanol (HFIP), trifluoroacetic acid (TFA), dimethyl sulfoxide (DMSO), tetramethylbenzidine, N,N-dimethylacetamide, bovine serum albumin (BSA, Fraction V), 30% w/w H2O2, silicon dioxide mesh (sand), polyethyleneglycol bisphenol A epichlorohydrin copolymer (PEG, 15-20kDa), rhodamine110 (R110) (Abs/Em maxima = 496/520 nm), urea, and guanidine hydrochloride (GdnHCl) were purchased from Sigma-Aldrich (St. Louis, MO). Sephadex G-75 and G-100 (medium) were purchased from GE Healthcare. N-α-biotinyl-Aβ(1-42) and fluorescein-Aβ(1–42) (Abs/Em=494/521nm) were purchased from Anaspec (San Jose, CA). Monoclonal Aβ (unmodified and biotinylated) antibodies to the human sequence Aβ-peptide, 4G8 (a.a. 17-24) were purchased from Covance Laboratories (Princeton, NJ). HRP-labeled streptavidin and HRP-goat antimouse secondary antibody were purchased from Rockland, Inc. (Gilbertsville, PA). NeutrAvidin (NA) was obtained from Pierce (Rockford, IL). High binding ELISA plates were obtained from Costar (Cambridge, MA). R-Phycoerythrin (Abs/Em maxima=546/578nm) was purchased from Invitrogen. Glass wool, 0.22μm syringe filter, Amicon ultra-15 centrifugal filter (50K cutoff) and phosphate buffered saline (PBS) 10x solution were purchased from Fisher Scientific (Waltham, MA) 9.9mm mica discs and 12mm metal specimen discs were obtained from Ted Pella (Redding, CA).

2.2 Sample Preparation

2.2.1 ELISA screening assays

2.2.1.1 Preparation of biotinyl-Aβ1-42 Oligomers

1 µl of 1 mg/ml N-terminal biotinyl-Aβ1-42 peptide dissolved in 1,1,1,3,3,3-hexa-fluoro-2-propanol (HFIP) solution was added to 25 µl additional HFIP in a polypropylene (PP) tube. HFIP was then removed with a gentle stream of inert gas creating a thin film of biotinylated Aβ peptide formed at the bottom of the PP tube. This film was subsequently dissolved in the same volume of trifluoroacetic acid (TFA) and then dried using an inert gas stream after incubation at room temperature for 10 min. An additional 25 µl of HFIP was added to redissolve the peptide film followed by HFIP removal along with any residual TFA using an inert gas stream. The treatment combined with HFIP and neat TFA aids in keeping Aβ1-42 monomeric by breaking up any "seeds" or small aggregates formed during storage. 70 µl of dimethyl sulfoxide (DMSO) was then added to dissolve the peptide film and after 10 min this 70 µl of 3 µM random coil peptide in DMSO was diluted 100-fold into oligomer-forming buffer (OFB = 50 mM sodium phosphate, 150 mM sodium chloride, pH 7.5) in a polypropylene container. After 30 min at room temperature, 70 µl of OFB containing 10% v/v Tween 20 was added to stop the assembly reaction and stabilize the Aβ1-42 oligomers. This 30 nM mixed monomer–oligomer solution was then either used immediately or frozen in aliquots at -75 ℃ for further use within 6 months.

2.2.1.2 Sephadex G-100 size exclusion chromatography (SEC)

A 10-ml pipette column was packed with Sephadex G-100 beads in oligomer-forming buffer (OFB) over a layer of sand and glass wool. The column was then equilibrated with OFB containing 0.1% Tween 20 filtered through 0.22 µm-pore-size filter. 250 µl of the mixture of

oligomeric and monomeric Aβ1-42 peptide solution was layered on the top of the column and eluted with OFB+0.1% Tween 20. 400 µl fractions were collected into a 96-well polypropylene plate (Costar) after the first 3 ml of void volume had been discarded. Collected fractions were frozen at −20°C for detection of oligomers as well as total Aβ peptide by ELISA.

2.2.1.3 Preparation of NeutrAvidin-coated plate

A 96-well ELISA plate was coated on the bottom of each well with 50 µl of 1 µg/ml NeutrAvidin™ (NA) in 10mM sodium phosphate (pH7.5), sealed with adhesive film, and stored at 4 ^{o}C overnight. Before use, the plate was blocked for 2 hours at room temperature by adding 200µl OFB containing 0.1% v/v Tween 20 to each well.

2.2.1.4 Sandwich biotin–avidin assay for Aβ1-42 oligomers

Aβ oligomers were assayed by biotin-avidin based interaction, which is less expensive than using antibodies and highly specific for recognition of oligomers [104]. As shown in Figure 2.1, NA immobilized on the plate surface captures both biotin-labeled monomers and oligomers. Only oligomers with exposed biotin are detected by HRP-labeled streptavidin (SA-HRP) allowing for the direct quantification of oligomers in the presence of monomeric peptide.

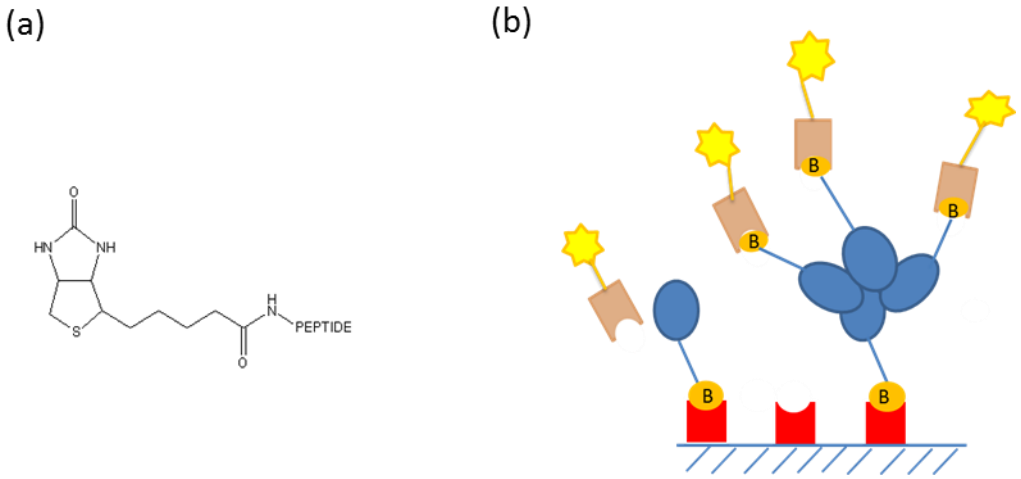

Figure 2.1. Configuration of single-site biotin–avidin assay for Aβ1-42 oligomers. a, Chemical structure of N-α-biotinyl-Aβ(1-42); b, NeutrAvidin™ (red) was immobilized on the surface of the plate to capture both biotin- labeled monomer and oligomer through the biotin-avidin interaction. The captured monomer has a single biotin that since it is bound to NA is unavailable to interact with HRP-labeled streptavidin to generate a signal. The oligomer can be detected by SA–HRP because it contains uncomplexed biotins.

The blocking solution was removed from the plate and 50 µl of each fraction eluted from Sephadex G-100 SEC was placed into each well of the NA-coated plate, the plate sealed, and incubated for 2 h at room temperature with shaking at 150 rpm. The plate was washed three times with 200 µl per well TBST (TBST = 20 mM Tris–HCl, 34 mM NaCl, pH 7.5, 0.1% Tween 20) with a Biotek ELx50 automated plate washer. To each well 50 µl of 1:20,000 SA–HRP in OFB containing 0.1% v/v Tween 20 was added. The plate was sealed, and incubated for 1 h at room temperature with shaking at 150 rpm. After incubation, the same washing steps were repeated and 100 µl tetramethylbenzidine (TMB)/H_2O_2 substrate solution was added [105]. After 5-10 min the reaction was stopped by adding 100 µl of 1% v/v sulfuric acid. The optical density (OD) of the solution in the wells which is proportional to the number of immobilized oligomers was measured at 450 nm using a Biotek Synergy HT plate reader.

2.2.1.5 Sandwich ELISA for total Aβ1-42 (monomer + oligomer)

For the total Aβ1-42 peptide assay, an NA-coated plate was used to capture biotinylated monomers and oligomers. The mouse monoclonal antibody, 4G8 which binds at a different site (Aβ residues 17-24), than the N-terminal biotin is added to bind to both monomers and oligomers. The bound 4G8 antibody is detected by HRP-goat anti-mouse secondary antibody (GAM–HRP) [104]. This total monomer + oligomer ELISA assay is depicted in Figure 2.2.

Similar to the oligomer assay, 50 µl of the sample fractions were added to each well of the NA-coated plate for total peptide assay, and incubated at room temperature for 2 h shaking at 150 rpm, and then washed three times. Wells were sequentially incubated for 1 h shaking at room temperature after adding 50 µl of 0.5 µg/ml 4G8 monoclonal antibody in OFB containing 0.1% Tween 20 and 2 mg/ml bovine serum albumin (BSA). Following washing, 50µl of 1:10,000 GAM–HRP in OFB – Tween-BSA was added, and the incubation was continued for 1 hr shaking at room temperature. The plate was washed and developed as for the oligomer assay. The activity of HRP was detected with TMB/H_2O_2 and the $OD_{450\ nm}$ was determined with a plate reader thus determining the total monomer + oligomer concentration. Combined with the oligomer assay described in 2.2.1.4, these assays allow for direct quantification of the monomer and oligomer concentrations in each sample fraction.

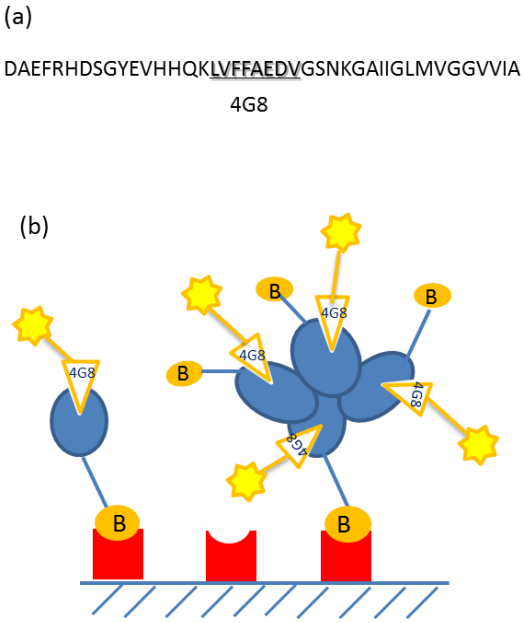

Figure 2.2. Configuration of single-site antibody assay for total Aβ1-42. a, Localization of 4G8 epitopes on the sequence of human Aβ(1-42). b, Binding to NA which was immobilized on the bottom of wells, biotin labeled monomer and oligomer were both recognized by antibody 4G8 to their 4G8 epitopes and the bound 4G8 antibody detected with GAM–HRP to generate a signal.

2.2.2 Fluorescence correlation spectroscopy experiment

2.2.2.1 Preparation of fluorescein-Aβ1-42 Oligomers

9.1µl of 0.2mg/ml fluorescein labeled Aβ1-42 (Fl–Aβ) monomer was mixed with 5.1µl of 1mg/ml wild type Aβ1-42 peptide into 25µL of HFIP, which was then removed with an inert gas stream. 500µl DMSO was added to dissolve the peptide film and the solution was vortexed every 5 min. After 15 min, the disaggregated peptide in DMSO was diluted 100-fold into 50ml OFB in a polypropylene tube and mixed thoroughly.

After 30 min, 2.5 ml of 1 mg/ml polyethyleneglycol bisphenol A epichlorohydrin (PEG,

15-20 kDa) copolymer filtered by 0.22 μm-pore-size filter was then added to the oligomer forming solution to stop the assembly reaction. The solution was then concentrated 6-fold by centrifugal filtration through a 50kDa cutoff membrane at 2, 500 xg at 4 ^{o}C in a swinging bucket rotor. 250 μl of this concentrated mixture of oligomeric and monomeric peptide was applied to the 10 ml Sephadex G100 column prepared as described in Section 2.2.1.3 and eluted with OFB + 0.1% v/v Tween 20. 400 μL fractions were collected with a 96-well polypropylene plate. Fluorescence intensity of each well was read by a Biotek Synergy HT plate reader. The isolated monomers and oligomers fractions would be distinguished by the peaks in the fluorescence intensity profile and further confirmed by fluorescence correlation spectroscopy (FCS) measurement.

The final volume of concentrated sample as well as the fraction of oligomers was determined to be proportional to the spin time. After concentration, residual monomer was washed through the filter by 2 ml OFB containing PEG15-20kDa, retaining the concentrated oligomers. In order to provide a sufficient number of oligomer 'events' for FCS experiments over a range of concentrations of Fl-Aβ in the sample, we concentrated our stock concentration of oligomers 100-fold. Concentrated solutions with high oligomer fractions were frozen in aliquots at -75 ^{o}C and diluted to appropriate concentrations for measurement by FCS.

2.2.2.2 PEG effect on concentration of Fl–Aβ oligomers solution

Oligomer solutions were prepared with and without PEG 15-20kDa following the same procedure described in Section 2.2.2.1 to determine the effect of PEG on oligomer formation. After concentration, final solutions were adjusted to a final volume of 500μl. After 30-fold dilution into phosphate buffered saline (PBS, 137 mM NaCl, 2.7mM KCl, 11.9mM phosphate buffer, pH7.4), 300μl of each sample was placed in a well of an 8-well NUNC chamber slide for FCS measurements.

2.2.2.3 Time course of FL-Aβ1-42 oligomer dissociation by FCS

The mixed oligomer-monomer FL-Aβ1-42 sample was diluted 30-fold from the concentrated oligomer stock solution into phosphate buffered saline (PBS) pH 7.4 and 300 µl pipetted into each sample chamber by. A series of DHBA isomers, which were effective oligomer dissociators previously determined by LeVine [103], were weighed and dissolved in Milli-Q water to make stock solutions 1mM, 0.5mM and 0.25mM, and then 3µl of each solution was added into individual 300µl diluted Aβ1-42 samples producing a final concentration of DHBA 10µM, 5µM and 2.5µM. Each chamber was measured by FCS at room temperature over time.

In addition, the effect of solvent (DMSO), a surfactant (Tween 20) and protein denaturants (urea and guanidine hydrochloride) on Aβ oligomer stabilities was also examined by FCS and compared to the DHBA isomers.

2.2.3Atomic Force Microscopy (AFM)

2.2.3.1 Preparation of sample for AFM

9.9 mm diameter mica discs were immobilized on 12 mm metal specimen discs with double–backed tape. For AFM experiments, a piece of single--sided Scotch tape was placed on the top of the mica surface and then gently peeled off to create a smooth, freshly cleaved surface suitable for force microscopy. 10 µl of the diluted Aβ samples solutions were deposited on the freshly cleaved mica and incubated for 15 minutes at room temperature. Samples were then rinsed with Milli-Q water for 10 seconds and gently blown dry under a stream of N_2 gas. When ready for imaging, each specimen disc was placed on top of the piezoelectric scanner of the AFM instrument.

2.3 Instrumentation

2.3.1 Fluorescence Correlation Spectroscopy

All FCS measurements were performed on an Alba FCS system (ISS) at room temperature. A Nikon Ti-U Epifluorescence microscope in an epi-illumination configuration with an apochromatic 60× numerical aperture 1.2 water immersion objective provided the focusing optics. The fluorescent particles were excited with the continuous wave 488 nm line from a solid-state diode laser and the emitted radiation was isolated by a 530 nm dichroic long pass filter. The intensity fluctuations were detected by an H7422-40 PMT detector (Hamamatsu) and the measured autocorrelation functions were analyzed and fit using a one or two component model with VistaVision software.

2.3.1.1 Theory of FCS

A well-defined observation volume typically on the order of femtoliters, defined as the "confocal volume", is formed by the laser passing through dichromic mirrors and objective of a confocal microscope. The lateral and axial dimensions, ω and z, for the confocal volume we used were determined to be approximately 3μm and 0.3μm, respectively (Figure 2.3a). The illumination volume is approximated with a three-dimensional Gaussian function and the calculated confocal volume is ~0.5 fL and the effective volume which is larger than the confocal volume by a factor of $2^{3/2}$, is equal to 4 fL [106]. When Brownian motion carries fluorescently labeled molecules through the confocal volume , the fluorescent dye is excited and emits fluorescence intensity F(t) detected using a photomultiplier tube (PMT) (Figure 2.3b). Fluctuations in the time correlation of the fluorescent signal is auto-correlated using VISTA software to calculate an autocorrelation curve [107]. The autocorrelation function G(τ) can be fit using model-dependent equations to reveal the mechanism and kinetics of the diffusion of the fluorescent particles; including the average number of fluorescent particles

and the average time that the particle takes to diffuse through the confocal volume. In this way, not only the size of the particles, but also the number concentration of particles can be determined by FCS [108]. Importantly, the relative fluctuations become smaller with increasing numbers of measured particles present in the confocal volume, so it is necessary to minimize the average number of particles for such an extremely small confocal volume. Therefore, an ideal working concentration for FCS measurement is one particle in the focal volume at a time, which typically results in solution concentrations of the order of nanomolar or lower for reliable fluctuation analysis [109].

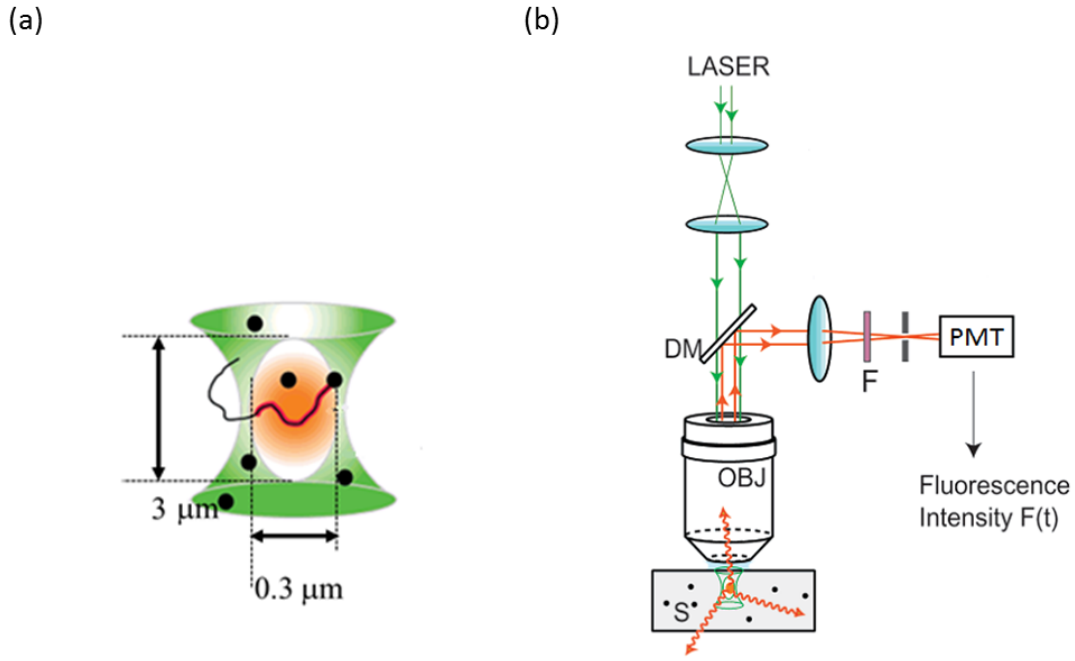

Figure 2.3. Confocal setup for FCS detection. Reprinted from reference: S.T. Hess, S. Huang, A.A. Heikal, W.W. Webb, Biological and chemical applications of fluorescence correlation spectroscopy: a review, Biochemistry 41 (2002) 697-705.

2.3.1.2 FCS data evaluation

FCS measures the temporal fluctuation in the fluorescence signal from the excited molecules in the confocal volume. The normalized autocorrelation function $G(\tau)$ of the intensity fluctuation $\delta F(t)$ of the signal $F(t)$ is defined as

$$G(\tau) = \frac{\langle \delta F(t)\, \delta F(t+\tau) \rangle}{\langle F(t) \rangle^2} \quad (1)$$

with

$$\delta F(t) = F(t) - \langle F(t) \rangle \quad (2)$$

where $\delta F(t)$ is the deviation of the intensity fluctuation [110]. Typically the illumination volume is approximated as a three-dimensional Gaussian function with lateral and axial dimensions, ω and z resulting in a 3D autocorrelation function of:

$$G_{3D}(\tau) = 1 + \frac{1}{N} \sum_{i=0}^{n} \left(\frac{1}{1+\frac{\tau}{\tau_D}} \right) \cdot \frac{x_i}{\sqrt{1+\frac{\omega^2}{z^2}\frac{\tau}{\tau_D}}} \quad (3)$$

where N is the average number of fluorescent particles and x_i is the fraction of particles with translational diffusion time τ_D [111,112]. Hence, the diffusion coefficient, D of particles can be determined by the beam waist, ω from the calibration with standard and τ_D, which describes the dwell time i.e. the average time particles remain in the confocal volume [110].

$$\tau_D = \frac{\omega^2}{4D} \quad (4)$$

In this study one-component as well as two-component systems were calculated and compared to mimic the monomeric Aβ solution and the mixed monomer-oligomer solution

with the assumption that both monomer and oligomer are, on average, spherical particles with distinct diffusion times.

For identical fluorescent particles undergoing ideal Brownian diffusion, dynamic information can be determined from the intensity fluctuations by means of a one component fit to the time autocorrelation given by

$$G(\tau) = 1 + \frac{1}{N}\frac{1}{\left(1+\frac{\tau}{\tau_D}\right)} \cdot \frac{1}{\sqrt{1+\frac{\omega^2}{z^2}\frac{\tau}{\tau_D}}} \tag{5}$$

If the system contains two diffusing species with sufficient hydrodynamic radii differences (e.g. a mixture of monomeric and oligomeric Fl-Aβ peptide), a two-component fit to the time auto-correlation can be used given by

$$G(\tau) = 1 + \frac{x_1}{N}\frac{1}{\left(1+\frac{\tau}{\tau_1}\right)}\frac{1}{\left(1+\frac{\omega^2}{z^2}\frac{\tau}{\tau_1}\right)^{1/2}} + \frac{x_2}{N}\frac{1}{\left(1+\frac{\tau}{\tau_2}\right)}\frac{1}{\left(1+\frac{\omega^2}{z^2}\frac{\tau}{\tau_2}\right)^{1/2}} \tag{6}$$

where x_1 represents the fraction of the monomeric Fl-Aβ with diffusion time τ_1, and x_2 represents the fraction of the oligomeric Fl-Aβ with diffusion time τ_2. x_1 and x_2 are dependent on quantum yield and average numbers of labeled Aβ species. While the quantum yield of oligomers and monomers are different (fluorescein-labeled oligomers are partially quenched) this does not affect this analysis since only the numbers of particles are being considered. Using equations (4) and (6), the diffusion coefficient, concentration and fraction of Fl-Aβ oligomers and monomers can be obtained from autocorrelation analysis. One limitation in single color FCS is there is a resolution limit for two-component systems as to the size differences required for meaningful data analysis. A resolution study of FCS measurement in 1999 [113] revealed that the distinction between two different molecular species depends strongly on their differences in size, brightness and concentration. In order to be distinguished, this study estimated that the diffusion times of two components must differ by at least a factor of 1.6 (i.e., a factor of ~4 difference in hydrodynamic volume for spherical particles).

One important assumption in this work is that both the Aβ peptide monomer and oligomer are spherical particles with constant diffusion coefficient or sizes over the time scale of the FCS measurement. Hydrodynamic radii r_h of each species can be calculated with the experimentally determined diffusion coefficient D by Stoke-Einstein equation:

$$r_h = \frac{k_B \cdot T}{6\pi\eta D} \tag{7}$$

where k_B is the Boltzman constant, T is the absolute temperature and η is the solvent viscosity. From this equation it is readily seen that the hydrodynamic radius, r_h of the particle is inversely proportional to the diffusion coefficient, D.

2.3.1.3 Optimization of measurement

300 μl of the samples were placed in an 8-well Laboratory-Tek chamber slide (Nalgene Nunc International). Three different concentrations, 2.5 nM, 5 nM and 10 nM of free rhodamine 110 (with known diffusion coefficient, D = 430 $\mu m^2 s^{-1}$) were used for calibrating z and ω, which are the axial and radial dimensions of confocal volume with the sampling time of 30 seconds in each measurement. Since the peptide was labeled with fluorescein, PBS was used as solvent to control ionization of the dye. Different sampling times and laser intensities were used for optimization of measurement conditions. In this study, 100 nM FL-Aβ1-42 sample (Abs/Em=494/521nm) was measured by FCS with 60% laser intensity and a short measurement time of 1min was used to minimize complications arising from photobleaching.

2.3.2 Atomic Force Microscopy

Aβ amyloid samples were characterized by a Park systems XE-70 atomic force microscope. All measurements were conducted in tapping mode with ultrasharp silicon cantilevers

NSC14/AIBS (MikroMasch), which contained a reflective aluminum backside coating and tip radius of ~10 nm. The typical resonant frequency of these NSC14/AIBS cantilevers was ~160 kHz with a force constant of 5.7 N/m. The Super Luminescence Diode (SLD) is used as the source for the 830nm laser. A scan size of up to 10 μm x 10 μm can be obtained by an X-Y scanner and a separate Z scanner with the XEP Software.

2.3.2.1 Theory of AFM

AFM uses a sensitive cantilever with a sharp tip to measure samples adsorbed on an atomically smooth surface [114]. When the AFM tip is scanning a surface, the cantilever bends due to forces between the tip and the sample surface which is dependent on the distance between them. A laser beam is aimed at the back of the cantilever and is reflected to a four-segment Position Sensitive Photo Detector (PSPD). The tube-shaped piezo scanner located under the sample monitors the movement of the sample in the horizontal direction by X-Y scan control and vertical direction controlled by the feedback loop. The measured cantilever deflections, containing the information of three dimensional shapes as well as the friction of the sample surface, allow a computer to generate an image of surface topography.

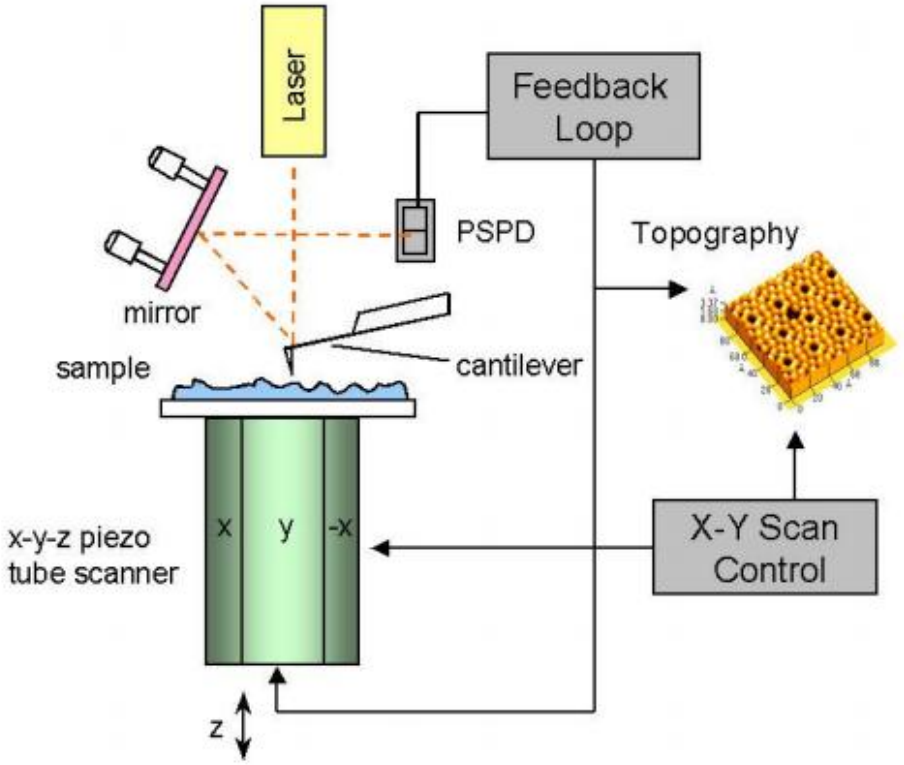

Figure 2.4. Schematic diagram of conventional AFM's working principle. Reprinted from reference: Park Systems Corp XE 70 User's Manual (2009)10.

2.3.2.1.1 Tapping mode imaging for Aβ peptide

There are two working modes in AFM: contact mode and tapping mode. During the contact mode scanning, a tip slides over the sample surface and is always in contact with the sample surface. Contact mode is especially useful for providing a high resolution for hard materials. The bend of the cantilever in the Y direction provides height information, and the distortion of the cantilever in the horizontal directions is indicative of the friction of the surface. However, the sliding of the tip may easily scrape the sample surface, especially for soft biological molecules.

Normally tapping mode is used for soft materials, like Aβ peptide [40]. In tapping mode, the cantilever is oscillated in a direction normal to the sample with constant oscillation amplitude associated with a feedback loop resulting in only intermittent contact with the surface [115]. Thus tapping mode avoids dragging the tip over the surface and protects the soft sample from tip damage. As shown in Figure 2.5, the amplitude of the oscillating tip decreases due to the repulsive force between the tip and the surface when it is scanning a higher surface region, e.g. oligomer adsorbed on the mica surface. Controlled by the feedback loop, a complementary voltage is applied to the Z scanner to lower down the sample in order to recover the amplitude so that the height information can be obtained from the voltage. Therefore, the topography images of the scanned surface can be acquired integrated with the lateral positioning information [116].

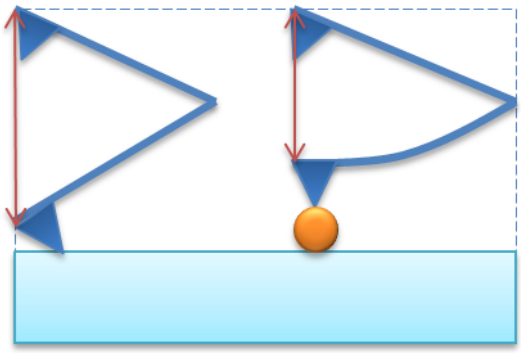

Figure 2.5. Schematic representation of detection of height in tapping mode. The oscillation amplitude of the cantilever decreases once the tip contacts a higher surface, e.g. oligomer peptide adsorbed on the mica surface.

Moreover, the interaction between the tip and the surface are very dependent on the moduli of the materials involved. When a tip interacts with a surface of different stiffness a phase shift occurs. The phase of the drive signal is compared with the phase of the cantilever response signal on the PSPD so that it is possible to distinguish between different materials by comparing the surface features from phase images, which might be barely visible in height or amplitude images [117].

Chapter Three: Results and Discussion

3.1 Detection of Aβ1-42 oligomers assembly

3.1.1 Fluorescence burst caused by Aβ1-42 assemblies

Monomeric Aβ1-42 dissolved in 1,1,1,3,3,3-hexafluoro-2-propanol (HFIP) and treated with neat trifluoroacetic acid to disrupt “seeds” and small aggregates, changes during the assembly process from random coil peptides into a mixture of monomers and oligomers following dilution from dimethyl sulfoxide (DMSO) into phosphate salt-rich oligomer forming buffer (OFB). This sample preparation method is a consistent way to achieve oligomeric Aβ1-42 with a total peptide concentration at biologically relevant (nanomolar) levels. The minimal concentration of total peptide for forming oligomers can be as low as 10 ng/ml (2.25nM) at room temperature as detected by an oligomer-specific single-site antibody assay [91].

For ELISA assay, Tween 20, a commonly used agent in ELISA assays to reduce background binding of antibodies, was added to block further aggregation assembly. For fluorescence correlation spectroscopy (FCS) measurements, PEG15-20kDa was used to inhibit aggregation as well as to block membrane adsorption during concentration of Aβ oligomers to obtain sufficient fluorescence intensity for oligomer detection in a reasonable time frame. Tween 20 forms micelles that are larger than 50kDa, so PEG15-20kDa was substituted to avoid concentrating the detergent. Figure 3.1 shows the fluorescence intensity of non-aggregated and aggregated fluorescein-Aβ1-42 solutions. Aβ1-42 oligomer-containing solutions display large fluorescence peaks in the raw data as shown in Figure 3.1b that are absent in monomer only solutions (Figure 3.1a). More bursts appear in the intensity traces when oligomer samples are concentrated by centrifugal filtration in the presence of PEG15-20kDa.

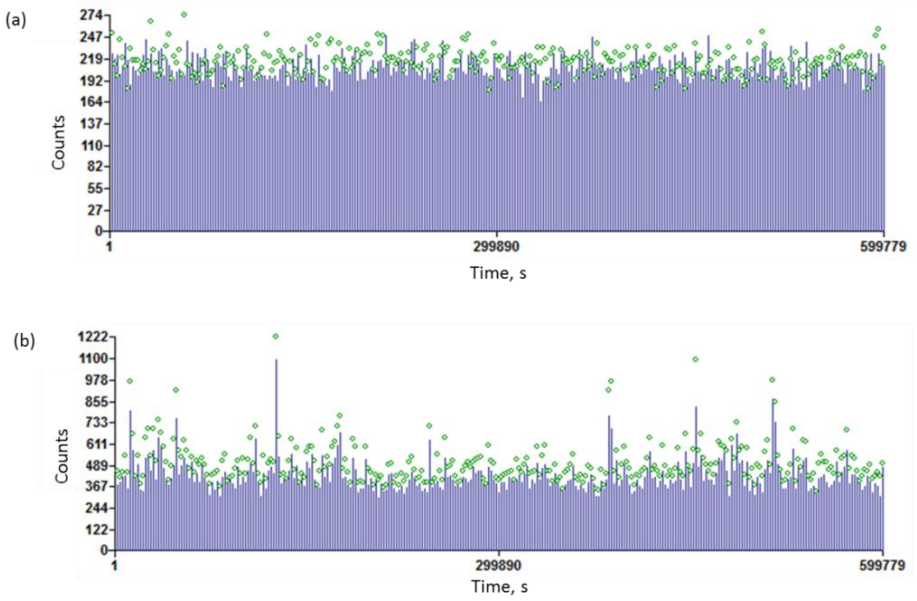

Figure 3.1. Fluorescence intensity traces (photon counts vs time (s)) of non-aggregated and aggregated Aβ1-42. Aβ oligomer samples were prepared by dissolving a mixture of the N-terminal fluorescein-labeled Aβ1-42 with wild type Aβ1-42 (1:4 mole/mole) in DMSO, before diluting in OFB. PEG15-20kDa was added after oligomer formation to prevent further assembly and to protect against peptide adsorption to the 50kDa m.w. cutoff filtration membrane used to separate oligomers from monomers and to concentrate the oligomers. (a) monomeric Aβ1-42 in the flow through of the centrifugal filtration; (b) the mixture of Aβ monomers and oligomers prepared after centrifugal concentration in the presence of PEG15-20kDa.

3.1.2 Size study of Aβ1-42 monomers and oligomers

3.1.2.1 Two-component fitting model

Unlike the monomeric Aβ sample (Figure 3.2a), the aggregated Aβ1-42 sample has an autocorrelation curve which cannot be well described with a one-component fit (red curve) given by equation 5 in the methods section in Chapter 2 . The blue curve is the result from a two-component fit (equation 6) described in the methods section. Here, we have modeled the data using a two-component fit where the fast component is fixed as the diffusion coefficient of monomeric Aβ1-42 and the slow component is allowed to vary. This approach results in

much better fitting than the one-component fit as shown in Figure 3.2b. The goodness

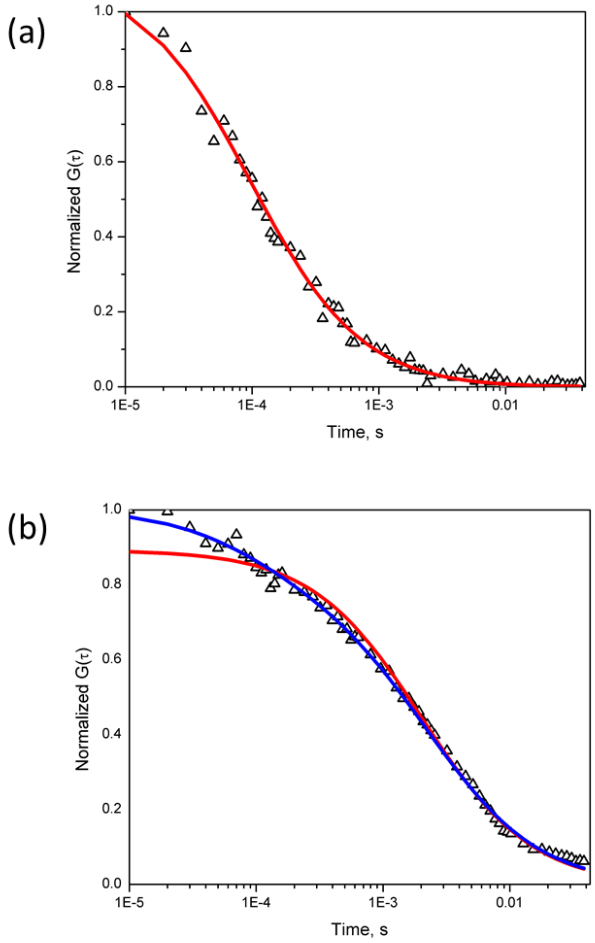

Figure 3.2. Fluorescence autocorrelation curves fit using one- and two-component fitting models for non-aggregated and aggregated Aβ1-42. (a) monomeric Aβ1-42 is well-described using a one-component fit shown in red; (b) mixed Aβ1-42 monomers and oligomers solutions are poorly described by a one-component fit (red curve) but are well-described with a two-component fitting (blue curve) where the diffusion coefficient for monomeric Aβ1-42 is fixed and another diffusion coefficient for a slower component describing the oligomeric fraction is allowed to vary. $\chi^2_{\text{(red curve)}}$=0.340, $\chi^2_{\text{(blue curve)}}$ =0.279.

of the selected model can also be checked against the acquired data by minimization of the χ^2 (chi-square) function using a Marquardt-Levenberg minimization algorithm. The value of χ^2 is generated by FCS data analysis software, VistaVision. χ^2 of the red curve from one-component fit, 0.340, is larger than χ^2 of the blue curve from two-component fit, 0.279. It

is, therefore, feasible to determine the diffusion coefficient, D_2 of oligomers as well as the fractions in the two-component fitting model with the D_1 of monomers fixed, determined from the autocorrelation curve of the monomer sample. For example, D_1 determined for monomer is 218 $\mu m^2/s$, so D_2 of oligomers can be determined from the blue autocorrelation function, which is 9 $\mu m^2/s$ with an oligomeric fraction of 77.6%.

We established a test system to determine the ability of our FCS system to distinguish diffusion of two non-interacting molecules of different molecular weights. Two fluorescent molecules, Rhodamine 110 (R110) and R-Phycoerythrin (PE), had their diffusion coefficients measured individually by FCS. Our measured values, 430 $\mu m^2/s$ and 48 $\mu m^2/s$ respectively, were similar to reference values [118]. The PE and R110 were mixed in different ratios (5:1, 3:1, 1:1, 1:3 and 1:5) and tested by FCS to verify the ability of FCS and our data analysis of the autocorrelation function to discern diffusion of two different-sized populations. The laser intensity applied was 60% and the sampling time was 5s in order to minimize the photobleaching effect on PE. The diffusion coefficients of R110 and PE were fixed for the analysis by the two-component fitting method. The fractions calculated for each probe from the fitting result were compared with the theoretical fractions due to mixing, are shown in Figure 3.3. Through statistical analysis with the chi square test, we calculate a p value (=0.9) much larger than 0.05 thus we cannot reject the hypothesis that there is no difference between observed fractions and theoretical fractions of two components at 0.05 significance level. Therefore, the experimentally determined fractions determined by FCS were consistent with the theoretical fractional mixture values of PE:R110 suggesting that the two-component fitting model was adequate to distinguish particles whose diffusion coefficients differ by 10 to 20-fold.

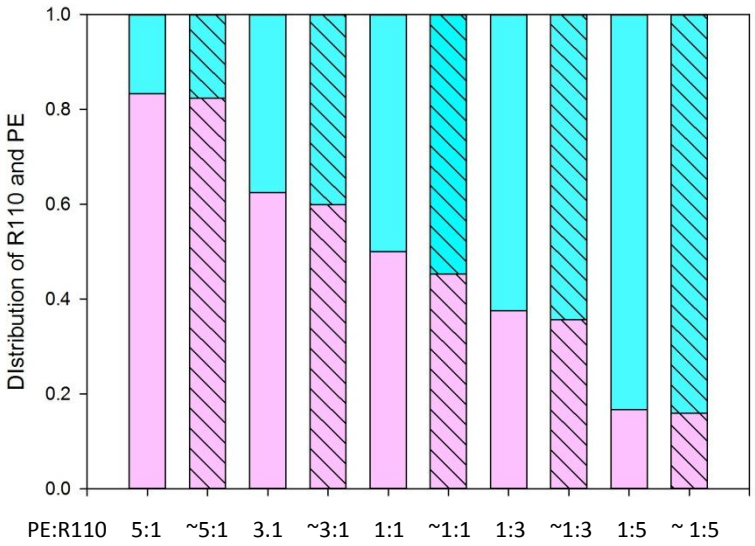

Figure 3.3. Evaluation of two-component fitting method with PE and R110 for FCS. The blue bars represent fractions of R110 and the pink bars are fractions of PE. The unhatched columns represent the mixed fraction of the two molecules and the hatched columns are the corresponding fractions calculated from the autocorrelation plot fits which are consistent with the proportions prepared in the mixture. (Statistical analysis result: The p value from chi square test is equal to 0.9, which is much larger than the significant level, 0.05, so the null hypothesis cannot be rejected)

3.1.2.2 Size characterization of Aβ1-42 monomers and oligomers

The stock solution of mixed Aβ1-42 monomers and oligomers was concentrated from 50ml OFB to 0.5 ml by centrifugal concentration through a 50kDa cutoff membrane. This stock Aβ1-42 solution enriched in oligomers was then diluted 30-fold into PBS for FCS measurement. Since most monomeric Aβ was removed by the molecular filtration, the final total Aβ concentration is much closer to physiological concentrations of Aβ than the ~μM concentration used in most prior studies [86,88,89] . This method of concentration provided Aβ concentrations that permitted consistent size evaluation of oligomer and sufficient detectable fluorescence intensity and sufficient number of oligomer ‘events’ for FCS experiments over a range of concentrations of Fl-Aβ in the sample. Autocorrelation curves can be obtained for various fluorescent species of different sizes.

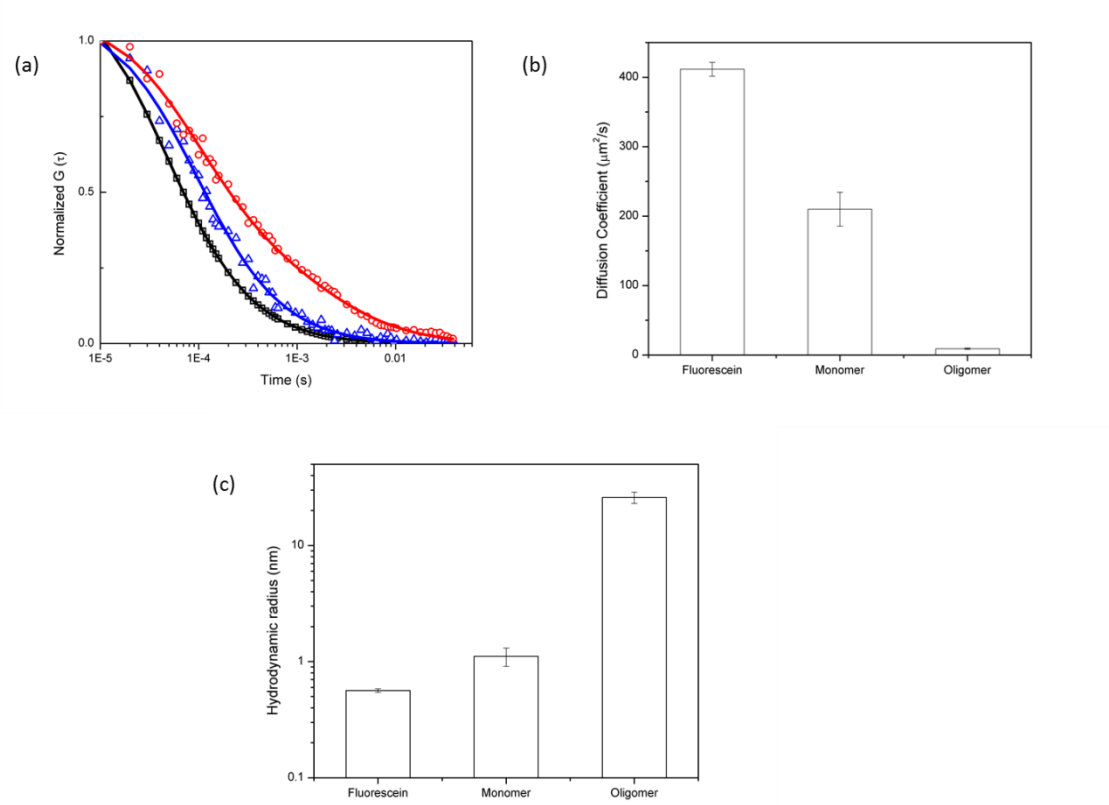

Figure 3.4. Fluorescence correlation of fluorescence dye, monomeric and oligomeric amyloid-β. (a) normalized autocorrelation curves of (from left to right) fluorescein (black), Aβ monomers (blue), and mixed monomers and Aβ oligomers (red); (b) measurement of diffusion coefficients: $D_{Fluorescein}$ = 412 ±10 μm^2/s, $D_{monomer}$ = 210 ±24 μm^2/s, $D_{oligomer}$ = 9 ±1 μm^2/s; (c) the corresponding hydrodynamic radii (r_h) calculated using Stoke-Einstein relation: $r_{h,Fluorescein}$ = 0.56 ±0.02 n, m$r_{h,monomer}$ = 1.1 ±0.2 nm, $r_{h,oligomer}$ = 25.9 ±2.9 nm.

With one-component and two-component fitting analysis of the normalized autocorrelation curves for fluorescein and fluorescein-labeled Aβ peptide, monomeric and oligomeric Aβ can be compared as shown in Figure 3.4a. With the assumption, described in Materials and Methods, that both the Aβ peptide monomers and oligomers are spherical particles with constant diffusion coefficient or sizes over the time scale of the FCS measurement, the translational diffusion coefficients (D) of each sample can be calculated from G(τ), and the hydrodynamic radii (r_h) can be calculated by using Stoke-Einstein relation given in equation 7. Hydrodynamic radii of $r_{h,fluorescein}$ = 0.56 ± 0.02 nm, $r_{h,monomer}$ = 1.1 ± 0.1 nm, $r_{h,oligomer}$ = 25.9 ± 2.9 nm were determined by FCS as shown in Figure 3.4b and 3.4c. The hydrodynamic radius of the standard dye molecule used here (Rhodamine 110) was previously published to be r_h =

0.54 nm ± 0.04 nm [118]. Both D and r_h values from our experiments are consistent with previously published data [119].

3.1.3 PEG effect on assembly of Fl–Aβ oligomers

3.1.3.1 PEG effect on concentration of Fl–Aβ oligomers solution

With the normal Aβ oligomer preparation method (dilution of Fl-Aβ + WT peptide from DMSO solution into OFB) only a small fraction of the Aβ is oligomeric in a 30nM sample. Because the proportion of oligomeric Aβ was small the observation time required for sufficient numbers of oligomers to diffuse through the fluorescence observation volume would be very long. Hence, an effective way to concentrate Aβ oligomers was devised for practical measurements of Aβ monomers and oligomers by FCS. A derivative of PEG, polyethyleneglycol bisphenol A epichlorohydrin copolymer (PEG, 15-20kDa) was coupled with centrifugal filtration through a 50kDa cutoff membrane to concentrate Aβ oligomers m.w. > 100,000 in OFB. PEG15-20kDa stops Fl–Aβ aggregation, and allows recovery of Aβ1-42 monomers and oligomers from a gel filtration column and keeps oligomers from binding to the filter material without itself being concentrated by the filter.

To determine the effect of PEG 15-20kDa on centrifugal concentration of Fl–Aβ oligomers through the 50 kDa filter, two oligomer samples (concentrated no PEG; with PEG15-20kDa) were prepared and diluted in phosphate buffered saline buffer (PBS, 137 mM NaCl, 2.7mM KCl, 11.9mM phosphate buffer, pH7.4). By FCS, oligomers were only found when concentrating in the presence of PEG15-20kDa. The observed fluorescence intensities were extremely low for the oligomer sample concentrated without PEG15-20kDa revealing the fact that there were few fluorescein labeled species remaining in the sample after concentration (Table 3.1). Moreover, no FCS evidence was observed for the existence of oligomers in the flow-through of the concentrator in the presence or absence of PEG 15-20kDa due to leakage through the filter membrane. The fluorescence intensity of Fl-Aβ monomer in the

flow-through for non-PEG sample was also lower than that of PEG15-20kDa sample.

Table 3.1. Average fluorescence intensity for monomer in the flow-through of centrifugal filtration and concentrated Fl-Aβ sample. Unit of average fluorescence intensity, counts per second.

	PEG15-20kDa	Non-PEG
Monomer in the flow-through	~1000	~800
concentrated Fl-Aβ oligomer solution	~2000	~800

These results suggest the oligomers concentrated without PEG stuck to the filter membrane during the centrifugal filtration. It appears that PEG15-20kDa with a bis-phenol A core to which is attached two different oxyethylene chains (Figure 3.5), has more favorable interactions with the amyloid peptide (or the filter) and is able to keep the peptide from adsorbing to the filter.

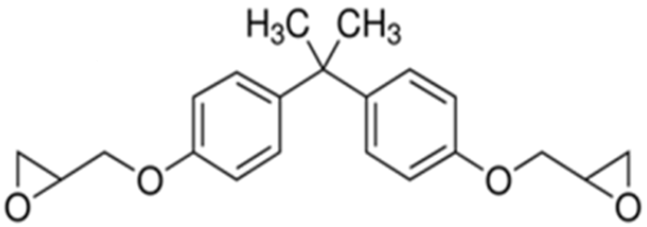

Figure 3.5. Chemical structures of a bis-phenol A core used to synthesize PEG15-20kDa.

3.1.3.2 PEG effect on the size of Fl–Aβ oligomers

Here arises a concern of whether adding PEG and concentration affect the size of oligomers. Atomic force microscopy (AFM) provided the ability to evaluate the morphology and

apparent size of oligomers and monomers. As one of a family of scanning probe microscope types, AFM is an ideal tool to follow the early events of Aβ amyloid assembly on single-molecule scale and used in this study to confirm the FCS result because it is capable of directly visualizing and measuring the dimensions of small protein that are adsorbed on the substrate from aqueous solution. However, AFM will only detect material that adsorbs to the substrate.

In order to study the effect of PEG15-20kDa on the size of Fl–Aβ oligomers, the concentrated Fl–Aβ oligomer sample was prepared with and without PEG15-20kDa and examined by AFM. The no PEG solution was obtained by direct dilution from DMSO to OFB with final total Aβ concentration of 100nM to avoid peptide being adsorbed on the filter membrane during centrifugal filtration. Fl–Aβ with PEG15-20kDa was diluted 30-fold from the stock solution as previously described and both solutions were immediately added to the mica surface for atomic force spectroscopy (AFM) measurement. The most accurate particle sizing is obtained by the height information recorded during tapping mode AFM. From the height analysis, we see that oligomers made without PEG were smaller than that made with PEG15-20kDa, and this difference matches with their hydrodynamic radii measurement by FCS.

As shown in Figure 3.6, the result shows that the average height of non-PEG sample is around 15nm which is much smaller than that of oligomer made with PEG15-20kDa (~45nm). The appearance of small particles with height of 2~3 nm, was observed in sample with PEG15-20kDa, while only a few can be found in the sample without PEG. In the phase images for samples formed with PEG15-20kDa , the observed oligomers appear to have a halo suggesting they might be covered with a different material with a modulus different than the Aβ peptide. Samples formed without PEG do not have this halo in the phase images. This data suggests that we may be observing the existence of a PEG coating in the PEG15-20kDa formed oligomers. To test this hypothesis, a control experiment was conducted by scanning the solvent containing the same concentration of PEG15-20kDa but without Fl–Aβ peptide and comparing the AFM images. As shown in Figure 3.7, only some ~3 nm particles were observed suggesting the thickness of PEG might interfere with the resolution of small peptide

like monomers/dimers in AFM. In addition, a halo as in the oligomeric Aβ PEG samples can be seen in the phase image, indicating the observation of PEG by AFM in both Aβ with PEG and PEG only sample. We conclude that the presence of PEG may affect both the ability to concentrate oligomers as well as their size. It is better to minimize the amount of PEG in the Aβ sample for AFM scanning in order to have a reliable definition of low-molecular-weight oligomers. The presence of PEG15-20kDa is also a concern in FCS experiments for determination of absolute diffusion coefficients of oligomers and monomers since the surface of Aβ is modified with PEG. However, in this study we are more focused on the relative change of sizes of oligomers in the presence and absence of assembly modulators and adding PEG15-20kDa is a necessary step to give us enough oligomers to detect by FCS diffusing through the observation volume in a short time.

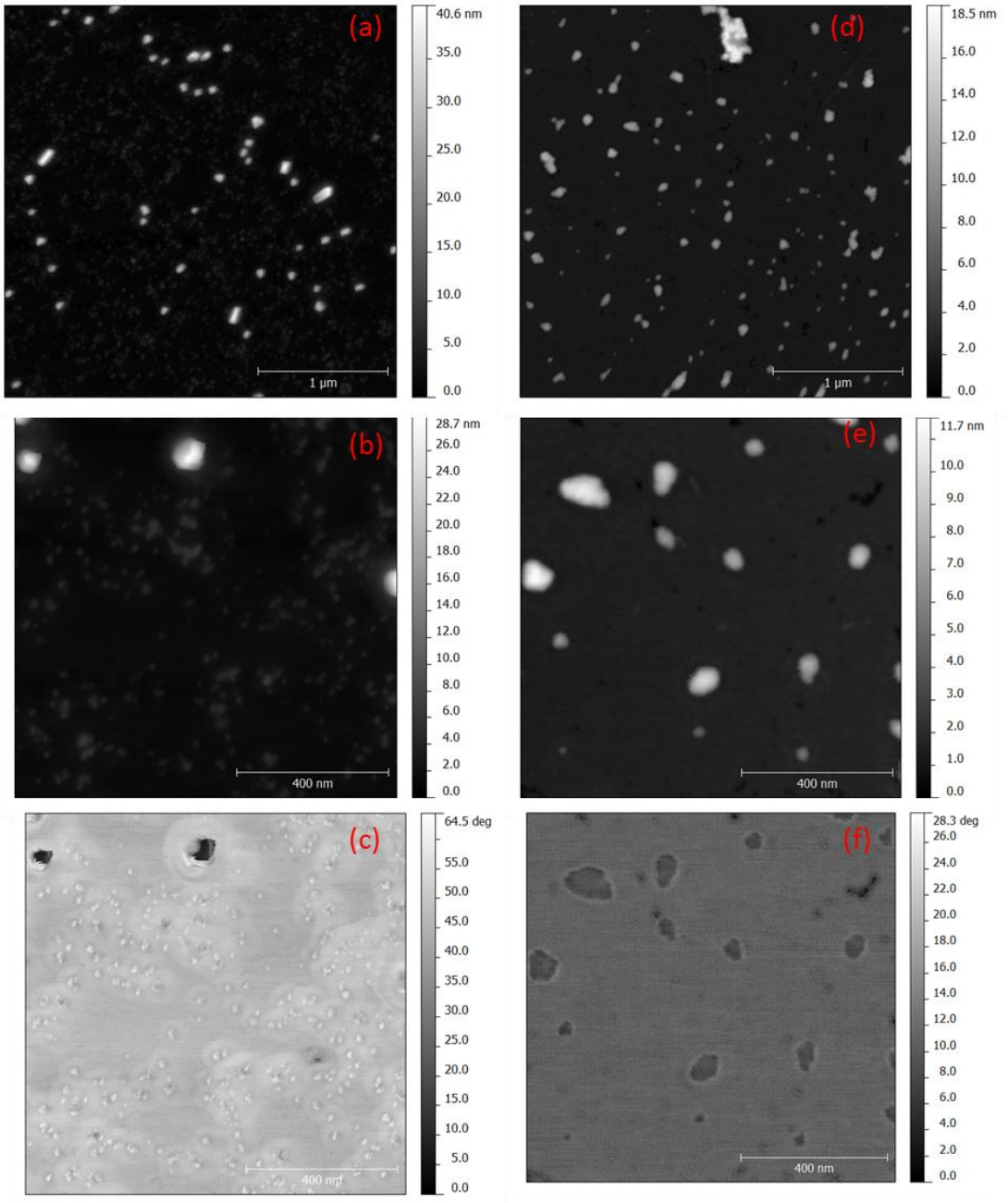

Figure 3.6. AFM of Fl-Aβ oligomer sample prepared w PEG15-20kDa and w/o PEG15-20kDa sample. a and b are topography images of Aβ1-42 oligomer sample w PEG15-20kDa and c is its phase image. d, e, and f are the topography images and phase images at the same sizes for Aβ1-42 oligomer sample w/o PEG15-20kDa. (scale bars: 1µm for a and d; 400nm for b, c, e, and f).

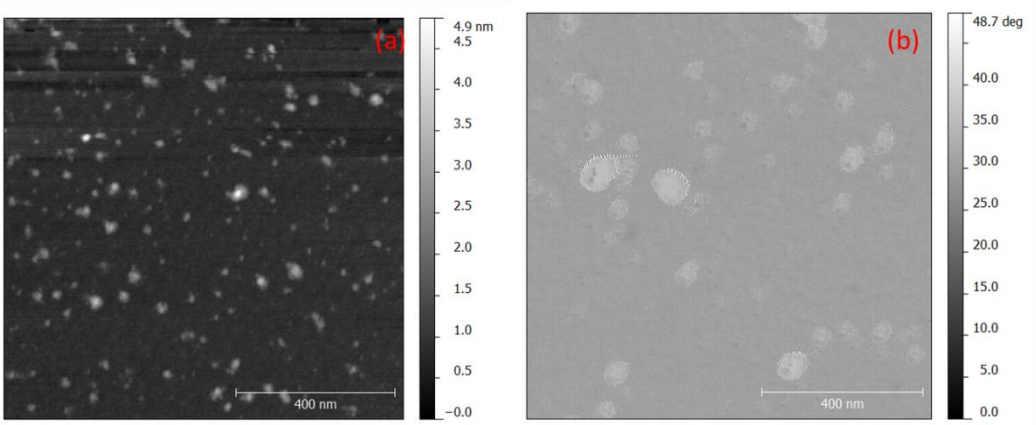

Figure 3.7. AFM of PEG15-20kDa solution. a, topography image of PEG15-20kDa solution; b, the corresponding phase image. (scale bars, 400nm)

3.2 Disassembly of oligomeric Fl–Aβ by small molecule dissociators of Aβ oligomers

To prepare the Fl-Aβ oligomer samples for FCS measurement, the mixed Aβ monomers and oligomers in oligomer forming buffer were concentrated by centrifugal filtration with a 50kDa cut off membrane in the presence of PEG15-20kDa and then stored in aliquots at -80 ^{o}C. Concentrated Fl-Aβ sample with high oligomer fractions were diluted 30-fold into PBS at the time of FCS measurement for the study of disassembly mechanism.

3.2.1 Kinetics of Aβ1-42 oligomer dissociation by DHBA isomers

A series of dihydroxybenzoic acid (DHBA) isomers were used to study the disassembly mechanism of soluble Aβ peptide oligomers. These molecules were selected based on previously published results by LeVine and coworkers [103] which established their structure-dependent efficacy to dissociate or stabilize Aβ1-42 oligomers after screening a small molecule structural diversity compound library. A primary dissociation experiment was carried out for (1:4) FL-Aβ/WT-Aβ incubated with 10 μM of each of the six DHBA isomers [103] and the relative changes in oligomer fraction were determined by FCS at 0h, 3h and 6h

(Figure 3.8). The oligomer fraction was determined by two-component fits to the FCS autocorrelation curves as described earlier. Only three isomers, 2,5-, 2,3- and 3,4- DHBA (Figure 3.9) were found to cause significant decrease of initial oligomer percentages and cause oligomer dissociation to monomer. Also, the difference between fractions of oligomers remaining in the solution for each DHBA isomers at the same time point reveals a possible difference between their dissociation potencies. These results are in good agreement with previously published results comparing oligomer and monomer fraction by sandwich ELISA assays [103]. These three active DHBA isomers were used to conduct the time course study of the disassembly mechanism of oligomers by FCS.

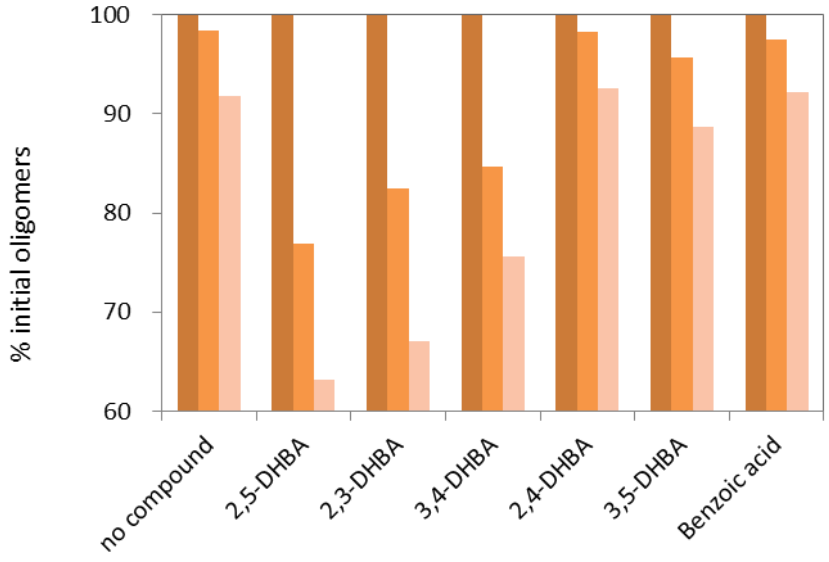

Figure 3.8. The percent of initial oligomers in the 100 nM Aβ oligomer solutions in the presence of all isomers of dihydroxybenzoic acid (DHBA) for incubation time of 0 h, 3 h and 6 h (from left to right). The concentration of compound in the solution was 10 μM.

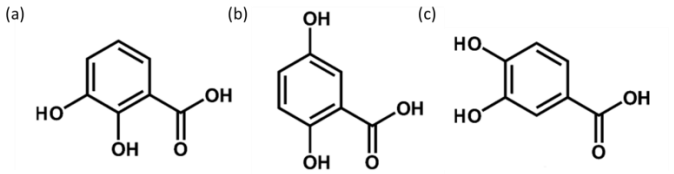

Figure 3.9. Chemical structures of active DHBA isomers for Aβ assembly dissociation. a, 2,3-DHBA; b, 2,5- DHBA; c, 3,4- DHBA.

The dissociating effect of 2,5-DHBA on oligomers is readily apparent from the increase of monomer fraction as shown in Figure 3.10. From this figure, we can observe two important kinetic phases; the intrinsic dissociation of oligomers and the compound-stimulated dissociation. The intrinsic dissociation of oligomer without any compound produced a single exponential decay; while the compound, 2,5-DHBA showed a concentration-dependent double-exponential decay behavior. The monomer fraction increases with increasing 2,5-DHBA concentration at each time point. All the 2,5-DHBA curves can be fit either by fixing D_1 of monomer as ~210 $\mu m^2/s$ and letting the D_2 vary or by fixing D_1 ~210 $\mu m^2/s$ and D_2 ~9 $\mu m^2/s$ (consistent with the FCS determined diffusion coefficient for monomer and oligomer respectively) resulting in similar monomer:oligomer fractions in both cases. Here the fraction of monomer grows over time at the expense of the fraction of oligomers. Surprisingly, the size of the remaining individual oligomers does not appear to change significantly over time. This data is consistent with a higher order dissociation process indicating that the dissociation mechanism is neither like fission of oligomers into intermediate size species, nor like dissociation of individual monomers from oligomers.

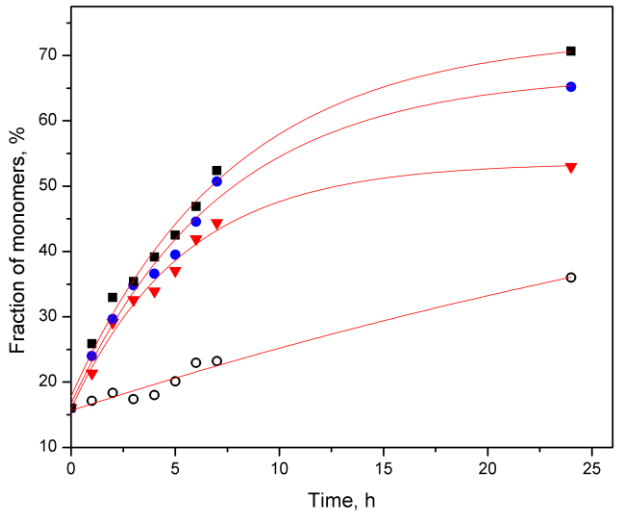

Figure 3.10. Time course of Aβ1-42 oligomer dissociation in the presence of 2,5-DHBA. Each data point represents the fraction of monomers after incubation of 100 nM Aβ1-42 (85% oligomers) for different times with a range of concentrations of 2,5-DHBA. No compound (open circle); 2.5 μM (closed inverted triangles), 5 μM (closed circles) and 10 μM (closed squares) 2,5-DHBA.

The less potent and efficacious 2,3- and 3,4-DHBA isomers also demonstrated their potencies to induce dissociation. Similar to 2,5-DHBA, their autocorrelation curves G(τ) can be well described by a two component fit with fixed diffusion coefficients of D_1 (~210 $\mu m^2/s$) and D_2 (~9 $\mu m^2/s$). As shown in Figure 3.11, these two DHBA isomers can also stimulate a double-exponential decay, which can be distinguished from the mono-exponential decay of intrinsic dissociation of the oligomers.

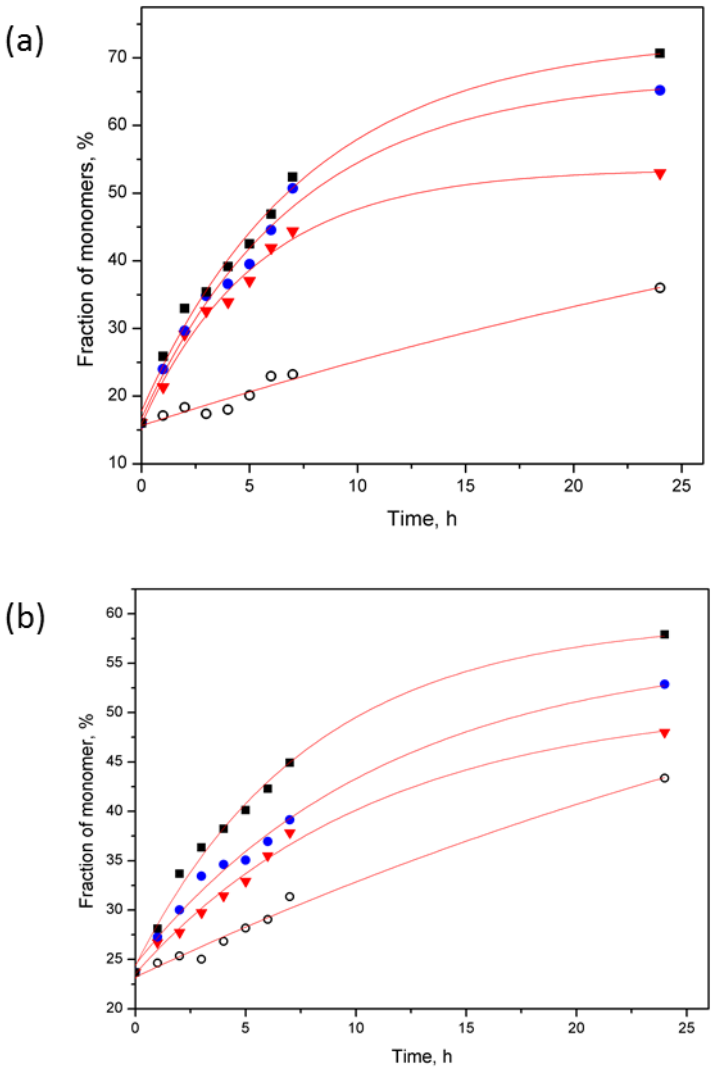

Figure 3.11. Time course of Aβ1-42 oligomer dissociation in the presence of (a) 2,3-and (b) 3,4-DHBA. Each data point represents the fractions of monomers after incubation of 100 nM Aβ1-42 (85% oligomers) for different times with a range of concentrations of 2,3- and 3,4-DHBA. No compound (open circle); 2.5 μM (closed inverted triangles), 5 μM (closed circle) and 10 μM (closed squares) 2,3-and 3,4-DHBA.

3.2.2 Similar dissociation results from FCS and ELISA

The different DHBA isomer effects on oligomers as measured by the FCS and ELISA methods may be compared when the fractions of oligomers remaining in the solution at different incubation time is extracted from each time course curve and normalized. Figure 3.12a shows the relative potencies of these 2,3-, 2,5-, and 3,4-DHBA isomers at 10 μM throughout the time course of Aβ oligomer dissociation. Interestingly, the trend is consistent with results from a time course study

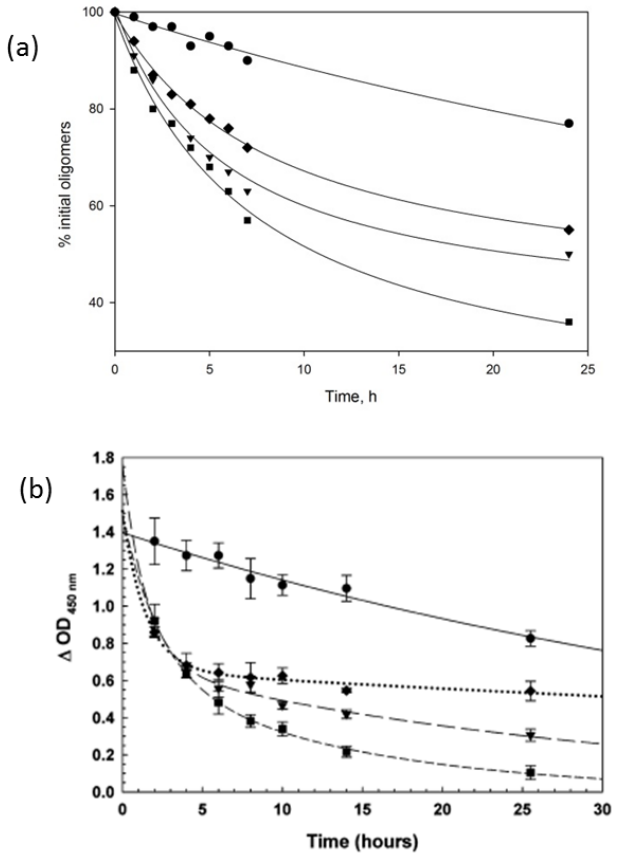

Figure 3.12. Effect of DHBA isomers on the time course of Aβ1-42 oligomer dissociation – comparison of FCS and ELISA methods. No compound (closed circle); 2.5μM (closed diamond), 5μM(closed inverted triangles) and 10 μM (closed squares) 2,3-and 3,4-DHBA. (a) Each data point represents the fractions of initial oligomers in the solution after incubation of 100nM Aβ1-42 (85% oligomers) for different times with 10 μM of 2,3- and 3,4-and 2,5-DHBA; (b) The amount of oligomers remaining after incubation for different times with 10μM of 2,3-, 2,5-, and 3,4-DHBA was determined by sandwich biotin–avidin assay with 2.8 nM biotinyl-Aβ(1-42) (from LeVine, et.al. [103]).

with the same DHBA isomers by sandwich biotin–avidin assay (Figure 3.12b) reported previously by LeVine [103]. 2,5-DHBA had the greatest dissociation potency and efficacy among the three active isomers. Two dissociation phases were observed by both techniques giving the impression of a double exponential decay process. One is an intrinsic dissociation of oligomers in the absence of compound which can be fit by a mono-exponential function; and the other provides an additional decay for interaction with DHBA isomers.

Importantly, there is no apparent size change of oligomers observed by FCS at any detection time during the dissociation process when reacted with DHBA isomers. This data is consistent with results in LeVine's previous study. No intermediates (<70kDa) of oligomers were detected by ELISA assay of SEC profiles at different times (0h, 2h, 5h and 8h) of dissociation caused by 2,5-DHBA.

3.2.3 Higher-order dissociation model

The fitting of correlation functions at different times with two fixed diffusion coefficients suggested there was no obvious change of size for oligomers during the dissociation process caused by DHBA isomers, which means the only two species detected in the solution were monomers and oligomers with constant sizes. One plausible hypothesis for the dissociation mechanism is that it is a higher-order dissociation process: a small molecule binds to an oligomer and stimulates its nearly instantaneous cooperative dissociation of oligomers into monomers. With the single-molecule level detection of freely diffusing species provided by FCS, the appearance of transient intermediates was not observed, consistent with a higher order cooperative dissociation process.

3.3 Vehicle (DMSO, Tween 20) effect on Aβ oligomer Disassembly

3.3.1 Different fractions of oligomers obtained from FCS and ELISA measurement

Size exclusion chromatography (SEC) is commonly utilized as a complementary method to study the size distribution of Aβ1-42 since there is a quantification caveat in the single site antibody assay that it is hard to distinguish between a large number of small oligomers and a small number of very large oligomers [120]. SEC separates particles based on their size (hydrodynamic radius); very large particles elute first in the void volume without penetrating the bead matrix while it takes longer for smaller molecules to enter and pass through the pores of the beads. Molecular weights of globular species by SEC can be calibrated in advance by comparing elution position to that of globular proteins of known sizes.

250 μL of 200 nM mixed Fl-Aβ monomers and oligomers (FAM:WT=1:4) prepared after centrifugal concentration was applied on a 12 ml Sephadex G100 column and eluted with OFB + 0.1% Tween 20. The fluorescence intensity profile for the collected fractions (Figure 3.13) showed two peaks distributed around Faction 5 and Fraction 23 indicating the position of fluorescein-labeled oligomers and monomers, respectively. Therefore, the 5 fractions centered around these two peaks was measured by FCS. Autocorrelation curves for fractions (5 ± 2 and 23 ± 2 nm), were consistent with isolated oligomer and monomer fractions, respectively. As shown in Figure 3.14, the curves for Fraction 23 and monomer in the filtration flow-through were identical and well described by a single component fit resulting in a diffusion time consistent with monomer. Fraction 5 was a mixture of oligomers and monomers and required a two-component fit to describe the autocorrelation function. The detected fraction of oligomers in Fraction 5, however, is only ~15%, which is different from the result obtained by our collaborator Dr. LeVine by re-running the pool of the void volume fractions from SEC containing oligomers on the Sephadex G100 SEC column again. Detecting total Aβ peptide the LeVine group saw very little monomer in the rechromatography (Figure 3.15).

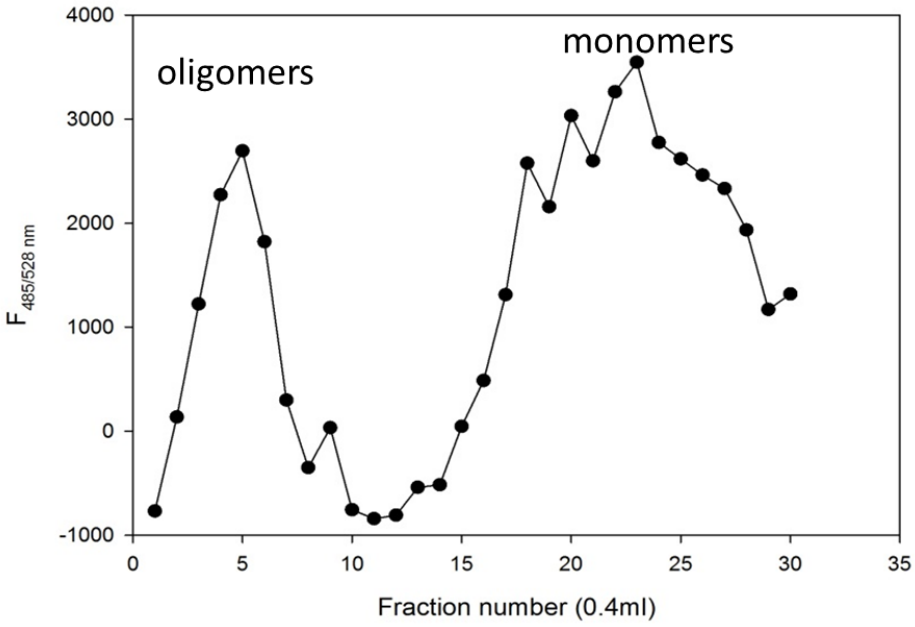

Figure 3.13. Fluorescence intensity profile for the elution of 200nM Fl-Aβ oligomer sample from Sephadex G100 size exclusion chromatography. Two hundred fifty microliters of 200nM Fl-Aβ mixed oligomers and monomer were applied to the column. After discarding three pre-void volume fractions (0.4ml), of thirty additional fractions were collected covering the Sephadex G100 column total bed volume as described in Method and Materials.

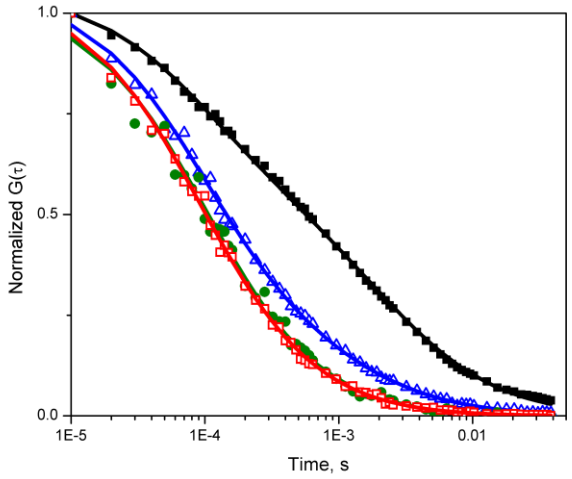

Figure 3.14. Fluorescence autocorrelation functions for the SEC pools (monomer and oligomer), monomer, and original 200 nM total Fl-Aβ sample. Monomers in the flow-through of the concentrator (closed circles), Fraction 23 (open squares), Fraction 5 (open triangles) and concentrated 200 nM Aβ solution (closed squares).

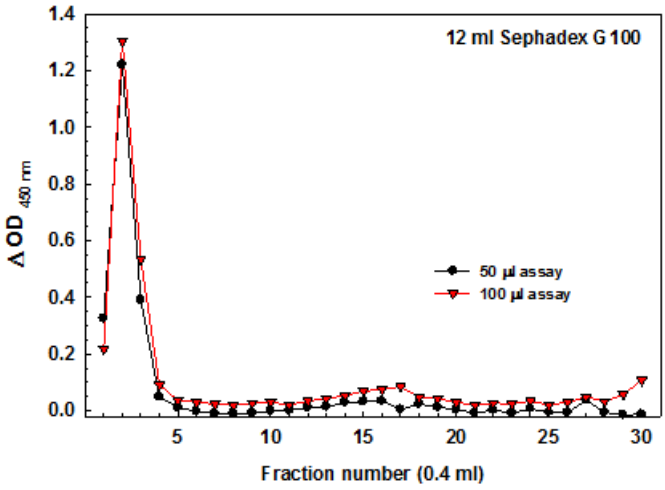

Figure 3.15. ELISA for total Aβ (6E10/bio4G8) of a re-run of Sephadex G100 void volume containing oligomers. There is maybe a hint of monomer around Fraction 15 but not as high as 85% monomer as reported by FCS. (made by Dr. LeVine)

According to FCS, Fraction 5 eluting in the column void volume with OFB+0.1% v/v Tween 20 should have a large fraction of oligomers. The autocorrelation fitting result from FCS shown in Figure 3.14, showed this sample to contain an even smaller fraction of oligomers (~15%) than the original concentrated total 200 nM Fl-Aβ mixtures (fraction of oligomers ~60%). The column fraction 5 solution contained 0.1% Tween 20 while the 200 nM Fl-Aβ mixtures were prepared in the presence of 100 µg/ml PEG15-20kDa without Tween 20. This caused us to explore the effect of solution conditions on the dissociation of Aβ oligomers. We do not have a satisfactory explanation why the high molecular weight fraction from SEC contained such a large proportion of monomer when examined by FCS.

3.3.2 Tween effect on Aβ oligomers disassembly

The mild detergent Tween 20 has been found to stabilize and inhibit oligomer formation at the early stages of complexation [91]. However, by FCS we find that pre-formed oligomers concentrated in the presence of PEG15-20kDa dissociate in the presence of Tween 20. Three different concentrations, 0.001%, 0.01% and 0.1%, of Tween 20 v/v were studied. 0.1% v/v Tween 20 is commonly used in the ELISA assay as well as the SEC separation to avoid adsorption of peptide and stop further assembly. The time course of concentration-dependent Aβ dissociation as measured by FCS is shown in Figure 3.16. The effect of Tween 20 can be observed in the initial rate dependence on Tween 20 concentration of monomer appearance

derived from the tangent to the early time course (Figure 3.17). This half-maximal effective concentration, EC_{50}, is approximately the critical micelle concentration of Tween 20 (~60 μM). Interestingly, as an oligomer assembly inhibitor, Tween 20 has been shown to block oligomer formation with an EC_{50} between 0.1 and 0.5 μM [121], much lower than 60 μM. Thus, at low concentrations Tween 20 appears to act as an oligomer assembly inhibitor, but at high concentrations it can induce dissociation of oligomers. Moreover, comparison of the FCS data suggests that both Tween 20 and DHBA isomers dissociate through a cooperative dissociation mechanism.

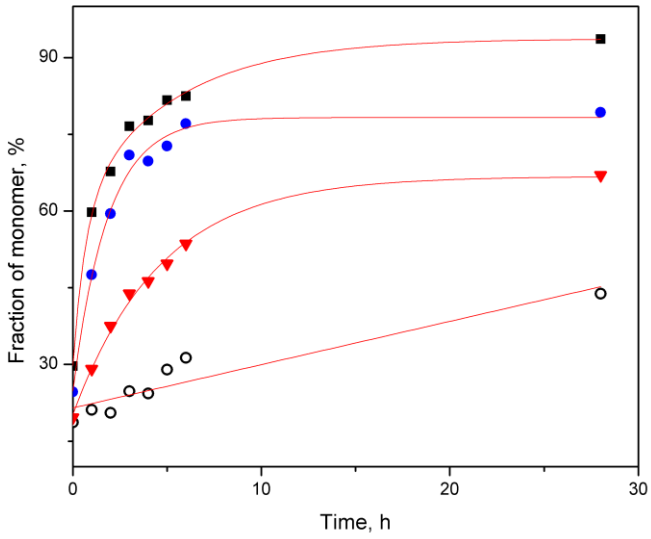

Figure 3.16. Time course of Aβ1-42 oligomer dissociation in the presence of Tween 20 over a range of concentrations. No Tween 20 (open circle); 0.001% (closed inverted triangles), 0.01% (closed circles), and 0.1% (closed squares) v/v Tween 20.

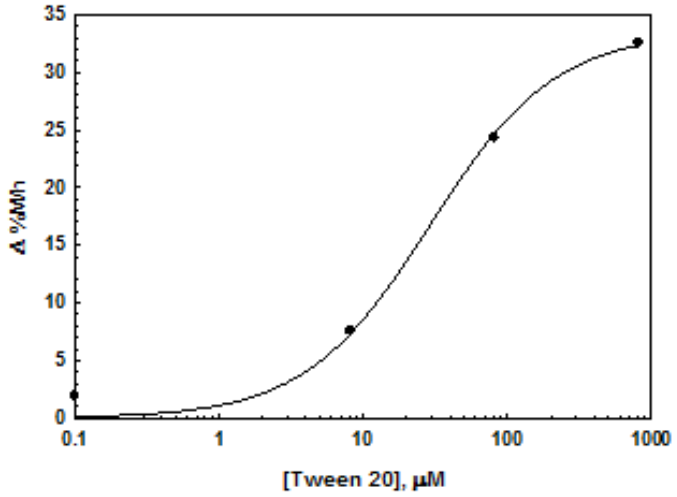

Figure 3.17. Initial rate of Aβ1-42 oligomer dissociation by Tween 20 at different concentrations.

3.3.3 DMSO effect on Aβ oligomers disassembly

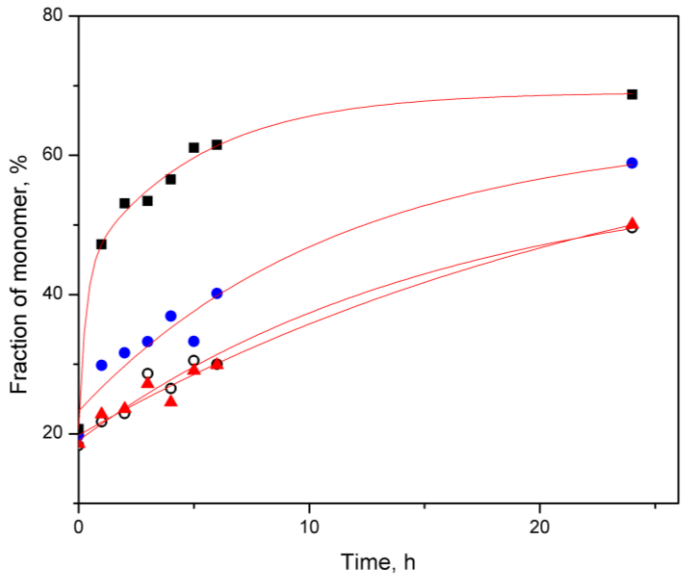

Figure 3.18. Time course of Aβ1-42 oligomer dissociation in the presence of DMSO. No DMSO (open circle), 0.1% v/v (closed inverted triangles), 0.7% v/v (closed circles), and 3% v/v (closed squares) v/v DMSO.

Aβ oligomer stability to the solvent DMSO was also examined by FCS as the solvent has been shown to both inhibit assembly and stimulate Aβ oligomer dissociation. Figure 3.18 shows that dissociation of Aβ1-42 oligomer is dependent on DMSO concentration. 0.1% v/v DMSO had little effect on dissociation and the curve was almost identical to the intrinsic dissociation curve (open circles). After adding 0.7% v/v DMSO the initial fraction of monomer at 0 h increased but the shape of the curve paralleled that of the intrinsic dissociation and 0.1% v/v DMSO curves. This suggests that these concentrations have similar dissociation rates. In the presence of 3% v/v DMSO the process became biexponential with time. The initial fraction of monomer increases, as well as the dissociation rate. For compound screening, DMSO is a convenient solvent capable of dissolving many compounds and minimizing their micelle/colloid formation which causes assay artifacts. Moreover, DMSO is used for monomer solubilization for Aβ oligomer preparation. From Figure 3.18, we see that while some DMSO is tolerated, too much DMSO (>3% v/v) severely affects the oligomer stability. Thus it is necessary to include a concentration control below 0.7% for DMSO. Similar to DHBA isomers as well as Tween 20, DMSO initiates the higher-order dissociation without generating detectable intermediate size oligomers.

3.4 Dissociation of Aβ oligomers by denaturants

Urea and guanidine hydrochloride (GdnHCl) are frequently used agents for destabilization of protein structure and denaturation of proteins. In this study, they were used to study self-quenching effects of fluorescein labelled oligomers by breaking up the oligomers completely into monomers and comparing the difference of the fluorescence counts compared to monomer:oligomer mixtures generated through exposure to Tween 20 and DMSO. In addition we found that these two denaturants favor a different dissociation mechanism than the higher-order cooperative dissociation previously discussed for Tween and the DHBA compounds.

3.4.1 Fitting models for Aβ oligomers exposed to urea and guanidine HCl denaturants

FCS autocorrelation curves measured after exposing Aβ oligomers to urea and GdnHCl were well described by a two-component fit with the fast component fixed to the measured diffusion coefficient of monomer similar to the previously described results. Unlike the Tween 20, DMSO and DHBA results, however, the slower diffusing species was not well described by differing proportions of oligomeric particles with fixed diameter. During the time course of disassembly caused by denaturants, our data indicates that both the fraction of oligomers and their size change over time. Figure 3.19c shows the FCS autocorrelation curve measured for oligomer samples treated with 8 M urea after 1h. As shown by the black curve, this autocorrelation is not well described by a model where D_1 and D_2 were fixed to the initial monomer and oligomer diffusion coefficients as for the control (Figure 3.19a) and the χ^2 for the black curve reached 0.558. As monomer size is fixed, we tried another model where we fixed D_1 and allowed D_2 to vary over time (blue curve, Fig 19c), which gave a larger D_2^* value with smaller χ^2, 0.313. This model accurately fits the autocorrelation curves consistent with a decrease in both size and number of oligomers as a function of time exposed to urea. Compared with to DMSO, for which the curve for 6 h DMSO treatment can still be described by fixing the same D_1 and D_2 as for control (Figure 3.19b), it is plausible that urea dissociates oligomers through a different dissociation mechanism than DMSO or DHBA.

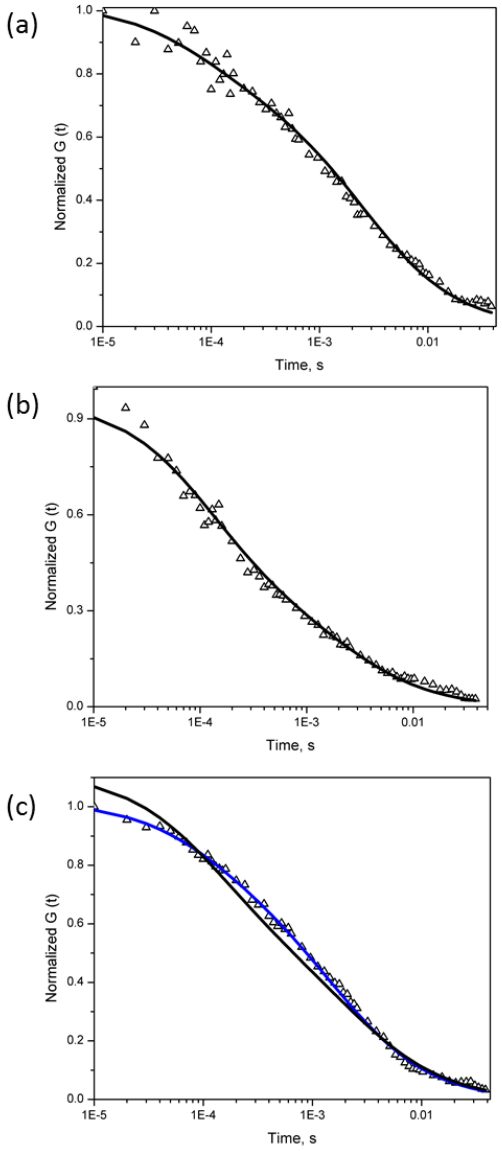

	D ($\mu m^2/s$)	r_h (nm)	Fractions, %
Monomer (D_1)	210	1.1	19.1
Oligomer (D_2)	10	23.3	80.9

	D ($\mu m^2/s$)	r_h (nm)	Fractions, %
Monomer (D_1)	210	1.1	63.5
Oligomer (D_2)	10	23.3	36.5

	D ($\mu m^2/s$)	r_h (nm)	Fractions, %
Monomer (D_1)	210	1.1	54.8
Oligomer (D_2)	10	23.3	N/A
Oligomer (D_2^*)	15	15.5	45.2

Figure 3.19. Comparison of different fitting results comparing DMSO and urea dissociation. (a), normalized autocorrelation function of control, Aβ containing 80.9% oligomers (r_h = 23.3 nm); (b), after 6 h incubation of 3% v/v DMSO; and (c), after 1h incubation of 8M urea. For (c), $\chi^2_{\text{(black curve)}}$=0.558, $\chi^2_{\text{(blue curve)}}$ =0.313.

3.4.2 Significant size change oligomer treatment with urea and GdnHCl

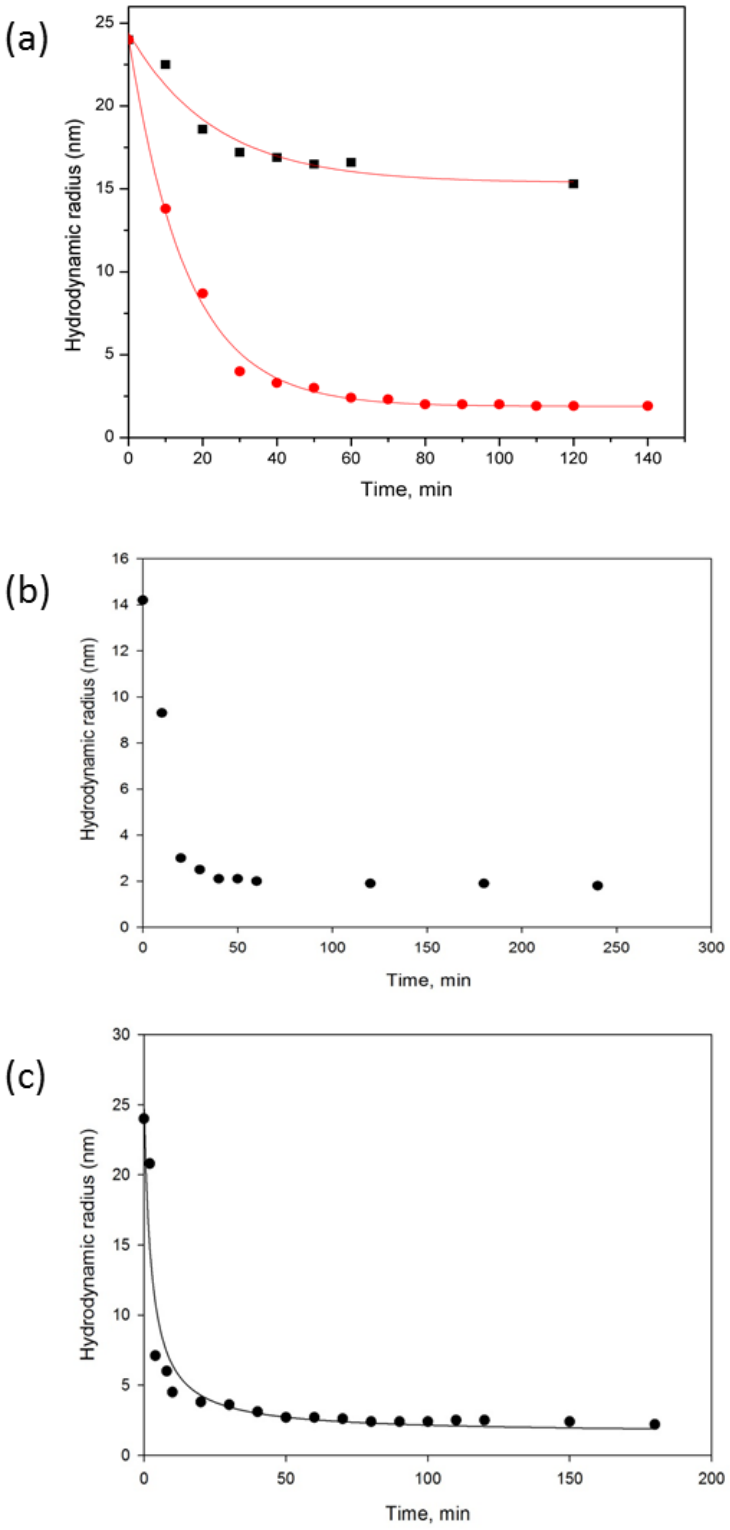

Figure 3.20. Hydrodynamic radius measurements of Fl-Aβ oligomers incubated with different denaturants as a function of time. a, 8 M urea (closed squares) and 8 M guanidine HCl (closed circle); b, adding 0.1% v/v Tween 20 after 19 h incubation with urea (urea-Tween-treatment); c, 8M urea + 0.1% v/v Tween 20.

The calculated hydrodynamic radius (r_h) is plotted as a function of time in Figure 3.20a. Urea treatment data is shown as closed squares, and GdnHCl is shown as closed circles. The urea treatment alone results in the rapid decrease of size of oligomers from 24.0nm to 15.3nm within 2h and then very slow decrease to 14.2nm between 2h to 19h. Dissociation by urea is incomplete. Addition of Tween 20 after 19 h incubation with urea induced significant decreases in size of the remaining oligomers from 14.2 nm to 2.0 nm within 45 min. The initial drop in the size was rapid and leveled out at r_h ~2 nm consistent with dimers. The appearance of intermediate, ~9.3 nm oligomers was observed within the first 10 min (Figure 3.20b), and the existence of similar intermediate of oligomer sizes (6 nm and 8.7 nm) was also observed for treatment of 8M GdnHCl. 0.1% Tween 20+ 8M urea, added together at time zero, induced much faster dissociation than urea alone and almost all the oligomers in the mixture broke up into ~2 nm within first 1h as seen in Figure 3.20c which are approximately the size of a dimer.

3.4.3 Understanding 2-3 nm species formation

For the lesser dissociation induced by 8M urea the fraction of monomer increased from 15% to 57% within 2 h while its size decreased from 24.0 nm to 15.3 nm. For the stronger dissociation by GdnHCl, Tween+urea, and Tween added after urea treatment (urea-Tween-treatment), the final products of dissociation were particles of 2-3 nm. FCS autocorrelation curves in these samples were well described by a simple one-component fit suggesting these 2-3 nm particles are the only remaining species in solution with no observed oligomers.

Focusing on the samples generated by urea-Tween-treatment, the 2-3 nm species may indicate that the multimeric oligomers (r_h = 24.0nm) were reduced into smaller oligomers (r_h = 14.2nm) after 19 h incubation with urea, and then adding the Tween changed the packing to give expanded monomers or dimer- or trimer species. However the reformation of dimers or

trimers containing at least one FL-Aβ from monomers where there are three non-fluorescent Aβ per one FL-Aβ would be relatively unlikely and the total concentration of fluorescent dimers should be relatively few.

The distinction between two different molecular species in FCS depends strongly on their differences in size as well as their relative concentrations, and the diffusion times of two components should differ by at least a factor of 1.6, or ~4x difference in hydrodynamic volume for spherical particles [113]. One hypothesis is that the appearance of a few dimers/trimers can interfere with the fitting result. This could explain why the FCS results showed that dimers/trimers were the only species left in the solution, but in fact there were much larger amount of monomers than dimers/trimers. Another hypothesis is there is a concentration-dependent effect for the transition between monomers and dimers/trimers. To test this hypothesis, we performed a dilution experiment to examine the effects of high oligomer concentration on FCS results. Four serial two-fold dilutions were carried out with products (~2.8 nm) after 22h of Tween+urea treatment. The measured size of the remaining particles decreased from 2.8 nm to 1.7 nm, indicating the high concentration of monomers dissociated from oligomers may induce a transition between monomers and dimers/trimers.

Also for the dissociation of oligomers by Tween 20 alone, we observed by FCS that the monomer fraction rose considerably. After 24h incubation, there were ~95% monomers compared to ~15% before adding Tween20. The remaining ~5% oligomers however were observed to have the same size as oligomers before the addition of Tween 20. Therefore, the disassembly process caused by urea and GdnHCl must differ from the previously observed higher-order cooperative dissociation induced by oligomer exposure to Tween 20, DHBA, and DMSO dissociation experiments. Urea and GdnHCl appear to proceed through a linear dissociation process where the fraction of monomers increases with time while the size of the oligomers simultaneously decreases.

3.5 Summary of Aβ oligomers disassembly mechanism

Current descriptions of Aβ oligomer assembly and disassembly mechanism are controversial. Most studies are focused on the assembly pathway in amyloid systems. In our study, two Aβ oligomer disassembly model are proposed, as described in Figure 3.21. Table 3.2 summarizes small molecule dissociators inducing different dissociation mechanisms and their working concentrations.

Table 3.2. Summary of dissociators studied in this thesis with different dissociation mechanisms and their working concentrations

Higher-order cooperative dissociation		Linear dissociation	
2,5-, 2,3- and 3,4-DHBA	10μM	Urea	8M
DMSO	3% v/v or 0.45M	GdnHCl	8M
Tween 20	0.1%v/v or 0.9mM		

A linear dissociation mechanism involving destabilizing of oligomer due to binding of small molecules, resulted in dissociation of monomer from oligomers with decreasing oligomer size (Figure 3.21a) has been hypothesized by several studies. The dissociation kinetics could be either mono- [81] or double-exponential [103] depending on the molecular structure of the dissociating molecules as well as their potency. In this study, we have directly observed this mechanism of dissociation caused by the protein denaturants urea and GdnHCl, by FCS at a single-particle level.

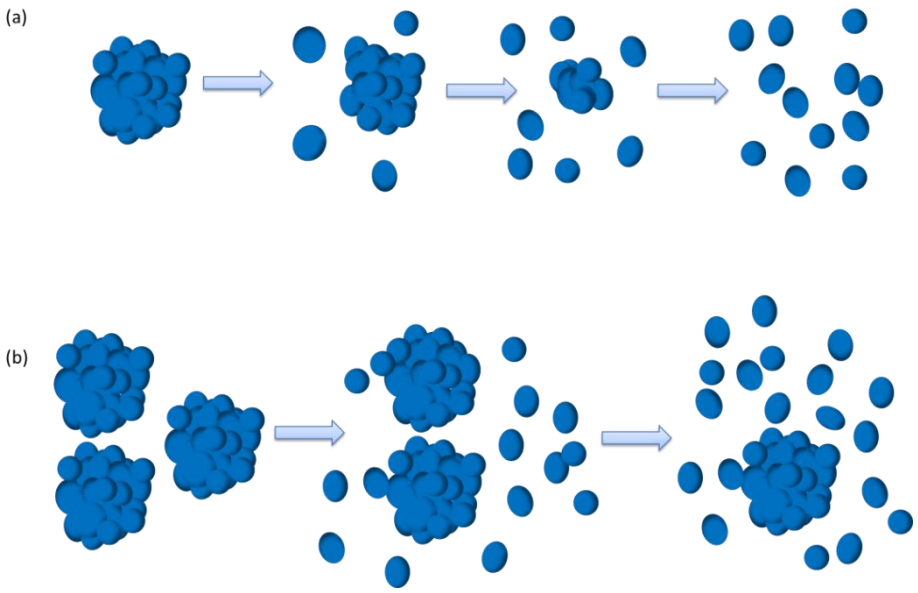

Figure 3.21. Schematic diagram of two proposed models for amyloid-β disassembly. a, linear dissociation; b, higher-order dissociation.

However, besides linear dissociation, another novel dissociation mechanism has been observed with Aβ oligomers exposed to certain DHBA isomers, DMSO, and Tween 20. For these molecules, we observe that the fraction of monomer increases at the expense of the fraction of oligomers. However, there is no accompanying change in apparent size of the remaining oligomers. This suggests a higher-order cooperative dissociation process where a nearly instantaneous dissociation of oligomers into monomers is stimulated by the active compound (Figure 3.21b). Compared with linear dissociation model, higher-order disassembly process seems more effective and potent for targeting oligomers since the oligomers are directly converted into nontoxic monomers without producing toxic intermediates with a significant half-life.

In summary, the application of a single-molecule methodology, FCS, provides unique insights and a facile way to monitor the Aβ assembly/disassembly pathway at physiological concentration. We studied the assembly kinetics of Aβ oligomers in the presence of different three active DHBA dissociators and evaluated their different potencies. The results show that

DHBA isomers, especially 2,5-DHBA, are prototypes for potential pharmaceutical agents for Aβ anti-oligomer therapy. They are relatively water-soluble small molecules of simple with strong efficacy to dissociate toxic synthetic Aβ oligomers directly into nontoxic monomers at a low dose. Two distinct dissociation models for soluble oligomeric amyloid-β were developed, of which the higher-order dissociation model provides a novel insight into drug design for treatment of preformed soluble Aβ assemblies in human brain.

Chapter Four: Conclusions and Future Work

4.1 Conclusions

In the current version of the amyloid cascade hypothesis soluble oligomeric Aβ peptide, rather than monomers or fibrils, is considered a primary etiologic agent for AD [122]. As the early event in AD pathologic process, the aggregation of Aβ triggers the downstream tau pathology, which is better correlated with dementia. Moreover, the formation of small similar oligomeric assemblies in other neurodegenerative disease such as Parkinson's disease, indicates that they could share a common mechanism of toxicity. Therefore it is important to investigate the assembly and disassembly kinetics of oligomers which are closely related to the amyloid-associated diagnosis and therapy of chronic neurodegenerative diseases.

Recently a sandwich biotin-avidin interaction based assay was developed to identify the assembly dissociation potency and efficacy of a series of dihydroxybenzoic acid (DHBA) isomers. However, whether there was formation of potentially toxic intermediates during the dissociation was unclear because this type of assay suffers from limited size information and oligomers with molecular weight below 40-50kDa are poorly detected.

The primary aim of this thesis was to harness a single-molecule detection method to provide an accurate quantification study of the assembly and disassembly mechanism of Aβ oligomers. Our hypothesis was that DHBA isomers enhance the dissociation of oligomers without forming potentially toxic intermediates, which was found to be supported by the results. The main achievements of this thesis are summarized as the following:

i) We successfully developed an effective single molecule method to study Aβ oligomer disassembly mechanisms.

The time course of Aβ1-42 oligomer dissociation at near physiological concentration was

investigated in the presence of DHBA isomers (2,5-, 2,3- and 3,4-DHBA) and other compounds. Using FCS, we investigated the size distribution of synthetic Aβ oligomers trace-labeled with fluorescein-tagged Aβ(1-42) and monitored in real time the change of size and mole fraction of oligomers in the presence of dissociating agents or conditions. With further confirmation by AFM, it provides the feasibility to evaluate the dissociation potency and efficacy of small molecules and to elucidate the specific dissociation mechanism.

ii) We elucidated a cooperative dissociation mechanism indicating that preformed Aβ oligomers are a possible therapeutic target and that small molecules can be found that dissociate oligomers without generating potentially toxic intermediate size oligomers.

This higher-order dissociation process with no transient oligomeric Aβ intermediates observed by FCS was first described in the thesis, indicating an avenue to effective anti-oligomer therapeutics. DHBA isomers are the first potent small molecules shown to stimulate such process. With a differential hydroxyl position-dependent ability, DHBA isomers dissociated preformed oligomers following a double-exponential decay kinetics, in agreement with the result from the ELISA assay [103].

iii) We identified at least two distinct Aβ disassembly pathways.

A linear dissociation mechanism with a progressive decrease of size and mole fraction of oligomers was observed when soluble oligomeric Aβ was exposed to the protein denaturants, urea and guanidine hydrochloride. The possibility of different disassembly pathways, one of which produces potentially toxic oligomeric intermediates, suggests that oligomer dissociation is responsive to ligand structure.

The advantages of FCS include high sensitivity, rapid analysis times, and minimal sample needed. However, there are still some limitations of the method such as the need to fluorescently label samples for measurement and low sample throughput. Assumptions of two components (oligomer and monomer) with constant spherical shape must be made. While the

Aβ concentration needed to provide a sufficient number of oligomer 'events' for FCS experiments over a range of ratios of Fl-Aβ:WT Aβ in the sample is more physiologically relevant than most previous experiments, it is still higher than known concentrations *in vivo*. Also, small changes in oligomer sizes would not be detectable by FCS. Hence, there is a continued need for improvement of this method in the future.

4.2 Future work

Understanding of the kinetics and disassembly mechanism of toxic oligomeric Aβ peptide will contribute to the development of therapeutic agents for treatment of amyloid aggregation in AD and possibly shed light on diagnostic approaches and therapeutic treatment of other neurodegenerative diseases. In order to thoroughly study the Aβ assembly-disassembly process, the employment of effective qualitative and quantitative methods is needed to provide a reliable detection of structure or size change of Aβ assemblies, and different molecular mechanisms induced by different chemotypes and at what stages those chemotypes act need to be clarified.

4.2.1 Follow time course of dissociation mechanism by atomic force microscopy, AFM

To complete this project, complementary AFM studies are needed to follow the time course of oligomer and monomer sizes and concentration. Due to the limitations of FCS discussed above, AFM could be utilized to correlate the mechanisms of protein aggregate dissociation suggested by FCS. AFM is capable of directly detecting and characterizing the morphology of Aβ aggregates in different sizes at near physiological concentration compatible with concentrations needed for FCS. Time course AFM studies would confirm the model-dependent results of oligomer dissociation observed by FCS. The smallest Aβ oligomers observed by conventional AFM was dimer (~4 nm) [123], thus AFM can solve the

resolution difficulties of FCS to distinguish between monomer and dimer/trimer Aβ.

Preliminary work with AFM was performed. By scanning the sample deposited on mica for AFM at different times of dissociation, the morphology was obtained and the changes of heights were compared with the FCS result. From the AFM topography images of Aβ oligomers treated with DMSO within first 1, 2, and 3 hours, the decrease of density of oligomers without change of height of oligomers was clear, which was consistent with the FCS result described in Chapter 3. These results show the promise of this complementary method, for monitoring time course studies of other small molecule dissociators, like DHBA isomers and Tween 20, as well as denaturants.

Some issues, however, about sample preparation need to be considered to improve the AFM images. For instance, in the denaturant dissociation experiments urea and GdnHCl readily recrystallized on the mica surface due to their high concentration (8M). Thus the mica samples need to be rinsed thoroughly to remove crystal artifacts on the mica which can be considered as “dirt” during scanning by AFM. More concerning, although also interesting is the possibility of surface coating of Aβ oligomers and the mica substrate by PEG15-20kDa , The PEG15-20kDa coating changes the dimensions of particles and may also interfere with binding of Aβ oligomers to the mica. One possible way to reduce the PEG concentration is washing through the spin column with oligomer forming buffer after the initial concentration with PEG present at the step of centrifugal concentration have coated the membrane filter.

4.2.2 Optimized FCS modeling and fitting method for linear dissociation model

Besides higher-order cooperative dissociation by DHBA isomers and Tween 20, a linear dissociation model was observed in the presence of protein denaturants, urea and GdnHCl suggesting a progressive release of monomers from oligomers with production of smaller oligomer intermediates. However, the simple two-component fit method for FCS data

analysis is inadequate for properly analyzing multi-component systems, such as multiple oligomeric intermediates of various sizes. An optimized modeling and fitting method needs to be developed.

A possible example or starting point for this is MEMFCS (maximum entropy method-base analysis of FCS data). This method analyzes FCS data in the model of a continuous distribution of diffusion species, and also seeks a maximum entropy distribution that is in agreement with all the experimental data [124]. The idea of maximum entropy has been widely used for image reconstruction from noisy and incomplete data, for which a general algorithm was first proposed by Skilling and Bryan [125]. For amyloid aggregation FCS studies, it has been applied to evaluate the stability of soluble Aβ oligomers at different pHs and ionic strength [126] and in the presence of divalent metal ions [88]. Hence, MEMFCS allows reliable descriptions of heterogeneous systems and can give an accurate quantification of numbers of oligomers of different sizes in a heterogeneous population, even though for highly complex specimens the method is time-consuming due to the massive computational requirement.

4.2.3 Study of a new oligomer assembly modulator: assembly inhibitors

The finding of linear dissociation model would not be “good news” for an oligomer targeting therapeutic due to the risk of forming toxic oligomeric intermediates. Previous study showed DHBA isomers have a hydroxyl position-dependent ability to dissociate preformed oligomers, but no have effect on assembly [103]. This is unlike clioquinol and other 8-hydroxyquinoline derivatives, which block oligomer formation at the stage of monomer or low n-mer formation [102]. Therefore, there are two different modes of oligomer assembly modulation, dissociation enhancers and assembly inhibitors which can be distinct. The former, which seems more promising, could target the oligomer which is already formed in the brain of AD patients to prevent AD or to slow down the progression of the disease.

Reference

[1] P.J. Muchowski, Protein misfolding, amyloid formation, and neurodegeneration: a critical role for molecular chaperones?, Neuron 35 (2002) 9-12.

[2] X.P. Wang, H.L. Ding, Alzheimer's disease: epidemiology, genetics, and beyond, Neurosci Bull 24 (2008) 105-109.

[3] H. Braak, E. Braak, Staging of Alzheimer-related cortical destruction, Int Psychogeriatr 9 Suppl 1 (1997) 257-261; discussion 269-272.

[4] S. Bonin-Guillaume, D. Zekry, E. Giacobini, G. Gold, J.P. Michel, [The economical impact of dementia], Presse Med 34 (2005) 35-41.

[5] N.L. Batsch, M.S. Mittelman, Overcoming the stigma of dementia, World Alzheimer Report 2012 Alzheimer's Disease International, London 2012, pp. 5.

[6] M. Hutton, J. Perez-Tur, J. Hardy, Genetics of Alzheimer's disease, Essays Biochem 33 (1998) 117-131.

[7] A. Alzheimer, About a peculiar disease of the cerebral cortex., Centralblatt für Nervenheilkunde Psychiatrie 30 (1907) 177–179.

[8] G.G. Glenner, C.W. Wong, Alzheimer's disease: initial report of the purification and characterization of a novel cerebrovascular amyloid protein, Biochem Biophys Res Commun 120 (1984) 885-890.

[9] G.G. Glenner, C.W. Wong, Alzheimer's disease and Down's syndrome: sharing of a unique cerebrovascular amyloid fibril protein, Biochem Biophys Res Commun 122 (1984) 1131-1135.

[10] J. Kang, H.G. Lemaire, A. Unterbeck, J.M. Salbaum, C.L. Masters, K.H. Grzeschik, G. Multhaup, K. Beyreuther, B. Muller-Hill, The precursor of Alzheimer's disease amyloid A4 protein resembles a cell-surface receptor, Nature 325 (1987) 733-736.

[11] A. Goate, M.C. Chartierharlin, M. Mullan, J. Brown, F. Crawford, L. Fidani, L. Giuffra, A. Haynes, N. Irving, L. James, R. Mant, P. Newton, K. Rooke, P. Roques, C. Talbot, M. Pericakvance, A. Roses, R. Williamson, M. Rossor, M. Owen, J. Hardy, Segregation of a Missense Mutation in the Amyloid Precursor Protein Gene with Familial Alzheimers-Disease, Nature 349 (1991) 704-706.

[12] J.A. Hardy, G.A. Higgins, Alzheimer's disease: the amyloid cascade hypothesis, Science 256 (1992) 184-185.

[13] B. Sommer, Alzheimer's disease and the amyloid cascade hypothesis: ten years on, Curr Opin Pharmacol 2 (2002) 87-92.

[14] J. Ghanta, C.L. Shen, L.L. Kiessling, R.M. Murphy, A strategy for designing inhibitors of beta-amyloid toxicity, J Biol Chem 271 (1996) 29525-29528.

[15] A. Lomakin, D.S. Chung, G.B. Benedek, D.A. Kirschner, D.B. Teplow, On the nucleation and growth of amyloid beta-protein fibrils: detection of nuclei and quantitation of rate constants, Proc Natl Acad Sci U S A 93 (1996) 1125-1129.

[16] S. Barghorn, V. Nimmrich, A. Striebinger, C. Krantz, P. Keller, B. Janson, M. Bahr, M. Schmidt, R.S. Bitner, J. Harlan, E. Barlow, U. Ebert, H. Hillen, Globular amyloid beta-peptide oligomer - a homogenous and stable neuropathological protein in Alzheimer's disease, J Neurochem 95 (2005) 834-847.

[17] C.G. Glabe, Structural classification of toxic amyloid oligomers, J Biol Chem 283 (2008) 29639-29643.
[18] M. Sakono, T. Zako, Amyloid oligomers: formation and toxicity of Abeta oligomers, FEBS J 277 (2010) 1348-1358.
[19] B. Soreghan, J. Kosmoski, C. Glabe, Surfactant properties of Alzheimer's A beta peptides and the mechanism of amyloid aggregation, J Biol Chem 269 (1994) 28551-28554.
[20] M.R. Sawaya, S. Sambashivan, R. Nelson, M.I. Ivanova, S.A. Sievers, M.I. Apostol, M.J. Thompson, M. Balbirnie, J.J. Wiltzius, H.T. McFarlane, A.O. Madsen, C. Riekel, D. Eisenberg, Atomic structures of amyloid cross-beta spines reveal varied steric zippers, Nature 447 (2007) 453-457.
[21] W.P. Esler, E.R. Stimson, J.M. Jennings, H.V. Vinters, J.R. Ghilardi, J.P. Lee, P.W. Mantyh, J.E. Maggio, Alzheimer's disease amyloid propagation by a template-dependent dock-lock mechanism, Biochemistry 39 (2000) 6288-6295.
[22] B. O'Nuallain, A.D. Williams, P. Westermark, R. Wetzel, Seeding specificity in amyloid growth induced by heterologous fibrils, J Biol Chem 279 (2004) 17490-17499.
[23] R.M. Koffie, M. Meyer-Luehmann, T. Hashimoto, K.W. Adams, M.L. Mielke, M. Garcia-Alloza, K.D. Micheva, S.J. Smith, M.L. Kim, V.M. Lee, B.T. Hyman, T.L. Spires-Jones, Oligomeric amyloid beta associates with postsynaptic densities and correlates with excitatory synapse loss near senile plaques, Proc Natl Acad Sci U S A 106 (2009) 4012-4017.
[24] C. Soto, L.D. Estrada, Protein misfolding and neurodegeneration, Arch Neurol 65 (2008) 184-189.
[25] P.J. Kahle, C. Haass, H.A. Kretzschmar, M. Neumann, Structure/function of alpha-synuclein in health and disease: rational development of animal models for Parkinson's and related diseases, J Neurochem 82 (2002) 449-457.
[26] H.Y. Zoghbi, H.T. Orr, Glutamine repeats and neurodegeneration, Annu Rev Neurosci 23 (2000) 217-247.
[27] A. Corsaro, S. Thellung, V. Villa, M. Nizzari, T. Florio, Role of prion protein aggregation in neurotoxicity, Int J Mol Sci 13 (2012) 8648-8669.
[28] M. Chattopadhyay, J.S. Valentine, Aggregation of copper-zinc superoxide dismutase in familial and sporadic ALS, Antioxid Redox Signal 11 (2009) 1603-1614.
[29] R. Kayed, E. Head, J.L. Thompson, T.M. McIntire, S.C. Milton, C.W. Cotman, C.G. Glabe, Common structure of soluble amyloid oligomers implies common mechanism of pathogenesis, Science 300 (2003) 486-489.
[30] P.T. Nelson, H. Braak, W.R. Markesbery, Neuropathology and cognitive impairment in Alzheimer disease: a complex but coherent relationship, J Neuropathol Exp Neurol 68 (2009) 1-14.
[31] P. Tiraboschi, L.A. Hansen, L.J. Thal, J. Corey-Bloom, The importance of neuritic plaques and tangles to the development and evolution of AD, Neurology 62 (2004) 1984-1989.
[32] M. Hutton, C.L. Lendon, P. Rizzu, M. Baker, S. Froelich, H. Houlden, S. Pickering-Brown, S. Chakraverty, A. Isaacs, A. Grover, J. Hackett, J. Adamson, S. Lincoln, D. Dickson, P. Davies, R.C. Petersen, M. Stevens, E. de Graaff, E. Wauters, J. van Baren, M. Hillebrand, M. Joosse, J.M. Kwon, P. Nowotny, L.K. Che, J. Norton, J.C.

Morris, L.A. Reed, J. Trojanowski, H. Basun, L. Lannfelt, M. Neystat, S. Fahn, F. Dark, T. Tannenberg, P.R. Dodd, N. Hayward, J.B. Kwok, P.R. Schofield, A. Andreadis, J. Snowden, D. Craufurd, D. Neary, F. Owen, B.A. Oostra, J. Hardy, A. Goate, J. van Swieten, D. Mann, T. Lynch, P. Heutink, Association of missense and 5'-splice-site mutations in tau with the inherited dementia FTDP-17, Nature 393 (1998) 702-705.

[33] E. Karran, M. Mercken, B. De Strooper, The amyloid cascade hypothesis for Alzheimer's disease: an appraisal for the development of therapeutics, Nat Rev Drug Discov 10 (2011) 698-712.

[34] L.L. Iversen, R.J. Mortishire-Smith, S.J. Pollack, M.S. Shearman, The toxicity in vitro of beta-amyloid protein, Biochem J 311 (Pt 1) (1995) 1-16.

[35] J.L. Price, D.W. McKeel, Jr., V.D. Buckles, C.M. Roe, C. Xiong, M. Grundman, L.A. Hansen, R.C. Petersen, J.E. Parisi, D.W. Dickson, C.D. Smith, D.G. Davis, F.A. Schmitt, W.R. Markesbery, J. Kaye, R. Kurlan, C. Hulette, B.F. Kurland, R. Higdon, W. Kukull, J.C. Morris, Neuropathology of nondemented aging: presumptive evidence for preclinical Alzheimer disease, Neurobiol Aging 30 (2009) 1026-1036.

[36] D. Games, D. Adams, R. Alessandrini, R. Barbour, P. Berthelette, C. Blackwell, T. Carr, J. Clemens, T. Donaldson, F. Gillespie, et al., Alzheimer-type neuropathology in transgenic mice overexpressing V717F beta-amyloid precursor protein, Nature 373 (1995) 523-527.

[37] S. Baglioni, F. Casamenti, M. Bucciantini, L.M. Luheshi, N. Taddei, F. Chiti, C.M. Dobson, M. Stefani, Prefibrillar amyloid aggregates could be generic toxins in higher organisms, J Neurosci 26 (2006) 8160-8167.

[38] C. Haass, D.J. Selkoe, Soluble protein oligomers in neurodegeneration: lessons from the Alzheimer's amyloid beta-peptide, Nat Rev Mol Cell Biol 8 (2007) 101-112.

[39] J. Wang, D.W. Dickson, J.Q. Trojanowski, V.M. Lee, The levels of soluble versus insoluble brain Abeta distinguish Alzheimer's disease from normal and pathologic aging, Exp Neurol 158 (1999) 328-337.

[40] M.P. Lambert, A.K. Barlow, B.A. Chromy, C. Edwards, R. Freed, M. Liosatos, T.E. Morgan, I. Rozovsky, B. Trommer, K.L. Viola, P. Wals, C. Zhang, C.E. Finch, G.A. Krafft, W.L. Klein, Diffusible, nonfibrillar ligands derived from Abeta1-42 are potent central nervous system neurotoxins, Proc Natl Acad Sci U S A 95 (1998) 6448-6453.

[41] D.M. Hartley, D.M. Walsh, C.P. Ye, T. Diehl, S. Vasquez, P.M. Vassilev, D.B. Teplow, D.J. Selkoe, Protofibrillar intermediates of amyloid beta-protein induce acute electrophysiological changes and progressive neurotoxicity in cortical neurons, J Neurosci 19 (1999) 8876-8884.

[42] D.M. Walsh, I. Klyubin, J.V. Fadeeva, W.K. Cullen, R. Anwyl, M.S. Wolfe, M.J. Rowan, D.J. Selkoe, Naturally secreted oligomers of amyloid beta protein potently inhibit hippocampal long-term potentiation in vivo, Nature 416 (2002) 535-539.

[43] S. Lesne, M.T. Koh, L. Kotilinek, R. Kayed, C.G. Glabe, A. Yang, M. Gallagher, K.H. Ashe, A specific amyloid-beta protein assembly in the brain impairs memory, Nature 440 (2006) 352-357.

[44] C.L. Masters, G. Simms, N.A. Weinman, G. Multhaup, B.L. McDonald, K. Beyreuther, Amyloid plaque core protein in Alzheimer disease and Down syndrome, Proc Natl Acad Sci U S A 82 (1985) 4245-4249.

[45] F. Prelli, E. Castano, G.G. Glenner, B. Frangione, Differences between vascular and

plaque core amyloid in Alzheimer's disease, J Neurochem 51 (1988) 648-651.
[46] D.L. Miller, I.A. Papayannopoulos, J. Styles, S.A. Bobin, Y.Y. Lin, K. Biemann, K. Iqbal, Peptide compositions of the cerebrovascular and senile plaque core amyloid deposits of Alzheimer's disease, Arch Biochem Biophys 301 (1993) 41-52.
[47] T. Saito, T. Suemoto, N. Brouwers, K. Sleegers, S. Funamoto, N. Mihira, Y. Matsuba, K. Yamada, P. Nilsson, J. Takano, M. Nishimura, N. Iwata, C. Van Broeckhoven, Y. Ihara, T.C. Saido, Potent amyloidogenicity and pathogenicity of Abeta43, Nat Neurosci 14 (2011) 1023-1032.
[48] H. Lewis, D. Beher, N. Cookson, A. Oakley, M. Piggott, C.M. Morris, E. Jaros, R. Perry, P. Ince, R.A. Kenny, C.G. Ballard, M.S. Shearman, R.N. Kalaria, Quantification of Alzheimer pathology in ageing and dementia: age-related accumulation of amyloid-beta(42) peptide in vascular dementia, Neuropathol Appl Neurobiol 32 (2006) 103-118.
[49] I. Youssef, S. Florent-Bechard, C. Malaplate-Armand, V. Koziel, B. Bihain, J.L. Olivier, B. Leininger-Muller, B. Kriem, T. Oster, T. Pillot, N-truncated amyloid-beta oligomers induce learning impairment and neuronal apoptosis, Neurobiol Aging 29 (2008) 1319-1333.
[50] E. Portelius, N. Bogdanovic, M.K. Gustavsson, I. Volkmann, G. Brinkmalm, H. Zetterberg, B. Winblad, K. Blennow, Mass spectrometric characterization of brain amyloid beta isoform signatures in familial and sporadic Alzheimer's disease, Acta Neuropathol 120 (2010) 185-193.
[51] H. Mori, K. Ishii, T. Tomiyama, Y. Furiya, N. Sahara, S. Asano, N. Endo, T. Shirasawa, K. Takio, Racemization: its biological significance on neuropathogenesis of Alzheimer's disease, Tohoku J Exp Med 174 (1994) 251-262.
[52] T. Shimizu, Y. Matsuoka, T. Shirasawa, Biological significance of isoaspartate and its repair system, Biol Pharm Bull 28 (2005) 1590-1596.
[53] R.O. Weller, Pathology of cerebrospinal fluid and interstitial fluid of the CNS: significance for Alzheimer disease, prion disorders and multiple sclerosis, J Neuropathol Exp Neurol 57 (1998) 885-894.
[54] M. Costanzo, C. Zurzolo, The cell biology of prion-like spread of protein aggregates: mechanisms and implication in neurodegeneration, Biochem J 452 (2013) 1-17.
[55] H.W. Wang, J.F. Pasternak, H. Kuo, H. Ristic, M.P. Lambert, B. Chromy, K.L. Viola, W.L. Klein, W.B. Stine, G.A. Krafft, B.L. Trommer, Soluble oligomers of beta amyloid (1-42) inhibit long-term potentiation but not long-term depression in rat dentate gyrus, Brain Res 924 (2002) 133-140.
[56] F. Kamenetz, T. Tomita, H. Hsieh, G. Seabrook, D. Borchelt, T. Iwatsubo, S. Sisodia, R. Malinow, APP processing and synaptic function, Neuron 37 (2003) 925-937.
[57] J.R. Cirrito, K.A. Yamada, M.B. Finn, R.S. Sloviter, K.R. Bales, P.C. May, D.D. Schoepp, S.M. Paul, S. Mennerick, D.M. Holtzman, Synaptic activity regulates interstitial fluid amyloid-beta levels in vivo, Neuron 48 (2005) 913-922.
[58] N. Yamamoto, E. Matsubara, S. Maeda, H. Minagawa, A. Takashima, W. Maruyama, M. Michikawa, K. Yanagisawa, A ganglioside-induced toxic soluble Abeta assembly. Its enhanced formation from Abeta bearing the Arctic mutation, J Biol Chem 282 (2007) 2646-2655.

[59] F.G. De Felice, P.T. Velasco, M.P. Lambert, K. Viola, S.J. Fernandez, S.T. Ferreira, W.L. Klein, Abeta oligomers induce neuronal oxidative stress through an N-methyl-D-aspartate receptor-dependent mechanism that is blocked by the Alzheimer drug memantine, J Biol Chem 282 (2007) 11590-11601.

[60] G.M. Shankar, B.L. Bloodgood, M. Townsend, D.M. Walsh, D.J. Selkoe, B.L. Sabatini, Natural oligomers of the Alzheimer amyloid-beta protein induce reversible synapse loss by modulating an NMDA-type glutamate receptor-dependent signaling pathway, J Neurosci 27 (2007) 2866-2875.

[61] M. Townsend, T. Mehta, D.J. Selkoe, Soluble Abeta inhibits specific signal transduction cascades common to the insulin receptor pathway, J Biol Chem 282 (2007) 33305-33312.

[62] E. Masliah, E. Rockenstein, I. Veinbergs, Y. Sagara, M. Mallory, M. Hashimoto, L. Mucke, beta-amyloid peptides enhance alpha-synuclein accumulation and neuronal deficits in a transgenic mouse model linking Alzheimer's disease and Parkinson's disease, Proc Natl Acad Sci U S A 98 (2001) 12245-12250.

[63] J. Lauren, D.A. Gimbel, H.B. Nygaard, J.W. Gilbert, S.M. Strittmatter, Cellular prion protein mediates impairment of synaptic plasticity by amyloid-beta oligomers, Nature 457 (2009) 1128-1132.

[64] H.B. Pollard, N. Arispe, E. Rojas, Ion channel hypothesis for Alzheimer amyloid peptide neurotoxicity, Cell Mol Neurobiol 15 (1995) 513-526.

[65] M. Kawahara, Y. Kuroda, Molecular mechanism of neurodegeneration induced by Alzheimer's beta-amyloid protein: channel formation and disruption of calcium homeostasis, Brain Res Bull 53 (2000) 389-397.

[66] N. Arispe, H.B. Pollard, E. Rojas, Giant multilevel cation channels formed by Alzheimer disease amyloid beta-protein [A beta P-(1-40)] in bilayer membranes, Proc Natl Acad Sci U S A 90 (1993) 10573-10577.

[67] H.A. Lashuel, D. Hartley, B.M. Petre, T. Walz, P.T. Lansbury, Jr., Neurodegenerative disease: amyloid pores from pathogenic mutations, Nature 418 (2002) 291.

[68] Y. Sokolov, J.A. Kozak, R. Kayed, A. Chanturiya, C. Glabe, J.E. Hall, Soluble amyloid oligomers increase bilayer conductance by altering dielectric structure, J Gen Physiol 128 (2006) 637-647.

[69] R. Kayed, Y. Sokolov, B. Edmonds, T.M. McIntire, S.C. Milton, J.E. Hall, C.G. Glabe, Permeabilization of lipid bilayers is a common conformation-dependent activity of soluble amyloid oligomers in protein misfolding diseases, J Biol Chem 279 (2004) 46363-46366.

[70] W.E. Klunk, R.F. Jacob, R.P. Mason, Quantifying amyloid beta-peptide (Abeta) aggregation using the Congo red-Abeta (CR-abeta) spectrophotometric assay, Anal Biochem 266 (1999) 66-76.

[71] H. LeVine, 3rd, Quantification of beta-sheet amyloid fibril structures with thioflavin T, Methods Enzymol 309 (1999) 274-284.

[72] N.E. Pryor, M.A. Moss, C.N. Hestekin, Unraveling the Early Events of Amyloid-beta Protein (Abeta) Aggregation: Techniques for the Determination of Abeta Aggregate Size, Int J Mol Sci 13 (2012) 3038-3072.

[73] I.A. Mastrangelo, M. Ahmed, T. Sato, W. Liu, C. Wang, P. Hough, S.O. Smith, High-resolution atomic force microscopy of soluble Abeta42 oligomers, J Mol Biol 358

(2006) 106-119.
[74] G. Bitan, M.D. Kirkitadze, A. Lomakin, S.S. Vollers, G.B. Benedek, D.B. Teplow, Amyloid beta-protein (A beta) assembly: A beta 40 and A beta 42 oligomerize through distinct pathways, Proceedings of the National Academy of Sciences of the United States of America 100 (2003) 330-335.
[75] H.A. Lashuel, P.T. Lansbury, Jr., Are amyloid diseases caused by protein aggregates that mimic bacterial pore-forming toxins?, Q Rev Biophys 39 (2006) 167-201.
[76] M. Hoshi, M. Sato, S. Matsumoto, A. Noguchi, K. Yasutake, N. Yoshida, K. Sato, Spherical aggregates of beta-amyloid (amylospheroid) show high neurotoxicity and activate tau protein kinase I/glycogen synthase kinase-3beta, Proc Natl Acad Sci U S A 100 (2003) 6370-6375.
[77] D.M. Walsh, A. Lomakin, G.B. Benedek, M.M. Condron, D.B. Teplow, Amyloid beta-protein fibrillogenesis. Detection of a protofibrillar intermediate, J Biol Chem 272 (1997) 22364-22372.
[78] C. Morgan, M. Colombres, M.T. Nunez, N.C. Inestrosa, Structure and function of amyloid in Alzheimer's disease, Prog Neurobiol 74 (2004) 323-349.
[79] A. Orte, N.R. Birkett, R.W. Clarke, G.L. Devlin, C.M. Dobson, D. Klenerman, Direct characterization of amyloidogenic oligomers by single-molecule fluorescence, Proc Natl Acad Sci U S A 105 (2008) 14424-14429.
[80] M. Cheon, I. Chang, S. Mohanty, L.M. Luheshi, C.M. Dobson, M. Vendruscolo, G. Favrin, Structural reorganisation and potential toxicity of oligomeric species formed during the assembly of amyloid fibrils, PLoS Comput Biol 3 (2007) 1727-1738.
[81] C.S. Gruning, S. Klinker, M. Wolff, M. Schneider, K. Toksoz, A.N. Klein, L. Nagel-Steger, D. Willbold, W. Hoyer, The Off-Rate of Monomers Dissociating from Amyloid-beta Protofibrils, J Biol Chem (2013).
[82] H. Ding, P.T. Wong, E.L. Lee, A. Gafni, D.G. Steel, Determination of the oligomer size of amyloidogenic protein beta-amyloid(1-40) by single-molecule spectroscopy, Biophys J 97 (2009) 912-921.
[83] M. Pitschke, R. Prior, M. Haupt, D. Riesner, Detection of single amyloid beta-protein aggregates in the cerebrospinal fluid of Alzheimer's patients by fluorescence correlation spectroscopy, Nat Med 4 (1998) 832-834.
[84] L.O. Tjernberg, A. Pramanik, S. Bjorling, P. Thyberg, J. Thyberg, C. Nordstedt, K.D. Berndt, L. Terenius, R. Rigler, Amyloid beta-peptide polymerization studied using fluorescence correlation spectroscopy, Chem Biol 6 (1999) 53-62.
[85] E. McGowan, F. Pickford, J. Kim, L. Onstead, J. Eriksen, C. Yu, L. Skipper, M.P. Murphy, J. Beard, P. Das, K. Jansen, M. Delucia, W.L. Lin, G. Dolios, R. Wang, C.B. Eckman, D.W. Dickson, M. Hutton, J. Hardy, T. Golde, Abeta42 is essential for parenchymal and vascular amyloid deposition in mice, Neuron 47 (2005) 191-199.
[86] G. Bitan, M.D. Kirkitadze, A. Lomakin, S.S. Vollers, G.B. Benedek, D.B. Teplow, Amyloid beta -protein (Abeta) assembly: Abeta 40 and Abeta 42 oligomerize through distinct pathways, Proc Natl Acad Sci U S A 100 (2003) 330-335.
[87] M. Duering, M.O. Grimm, H.S. Grimm, J. Schroder, T. Hartmann, Mean age of onset in familial Alzheimer's disease is determined by amyloid beta 42, Neurobiol Aging 26 (2005) 785-788.

[88] K. Garai, P. Sengupta, B. Sahoo, S. Maiti, Selective destabilization of soluble amyloid beta oligomers by divalent metal ions, Biochem Biophys Res Commun 345 (2006) 210-215.
[89] G. Bitan, A. Lomakin, D.B. Teplow, Amyloid beta-protein oligomerization: prenucleation interactions revealed by photo-induced cross-linking of unmodified proteins, J Biol Chem 276 (2001) 35176-35184.
[90] D.J. Selkoe, Normal and abnormal biology of the beta-amyloid precursor protein, Annu Rev Neurosci 17 (1994) 489-517.
[91] H. LeVine, 3rd, Alzheimer's beta-peptide oligomer formation at physiologic concentrations, Anal Biochem 335 (2004) 81-90.
[92] M.P. Murphy, T.L. Beckett, Q. Ding, E. Patel, W.R. Markesbery, D.K. St Clair, H. LeVine, 3rd, J.N. Keller, Abeta solubility and deposition during AD progression and in APPxPS-1 knock-in mice, Neurobiol Dis 27 (2007) 301-311.
[93] E.R. Siemers, R.A. Dean, R. Demattos, P.C. May, New pathways in drug discovery for Alzheimer's disease, Curr Neurol Neurosci Rep 6 (2006) 372-378.
[94] M.R. Farlow, NMDA receptor antagonists. A new therapeutic approach for Alzheimer's disease, Geriatrics 59 (2004) 22-27.
[95] L.S. Schneider, K.S. Dagerman, J.P. Higgins, R. McShane, Lack of evidence for the efficacy of memantine in mild Alzheimer disease, Arch Neurol 68 (2011) 991-998.
[96] B. Solomon, R. Koppel, E. Hanan, T. Katzav, Monoclonal antibodies inhibit in vitro fibrillar aggregation of the Alzheimer beta-amyloid peptide, Proc Natl Acad Sci U S A 93 (1996) 452-455.
[97] J. McLaurin, R. Cecal, M.E. Kierstead, X. Tian, A.L. Phinney, M. Manea, J.E. French, M.H. Lambermon, A.A. Darabie, M.E. Brown, C. Janus, M.A. Chishti, P. Horne, D. Westaway, P.E. Fraser, H.T. Mount, M. Przybylski, P. St George-Hyslop, Therapeutically effective antibodies against amyloid-beta peptide target amyloid-beta residues 4-10 and inhibit cytotoxicity and fibrillogenesis, Nat Med 8 (2002) 1263-1269.
[98] H. Hillen, S. Barghorn, A. Striebinger, B. Labkovsky, R. Muller, V. Nimmrich, M.W. Nolte, C. Perez-Cruz, I. van der Auwera, F. van Leuven, M. van Gaalen, A.Y. Bespalov, H. Schoemaker, J.P. Sullivan, U. Ebert, Generation and therapeutic efficacy of highly oligomer-specific beta-amyloid antibodies, J Neurosci 30 (2010) 10369-10379.
[99] I. Klyubin, D.M. Walsh, C.A. Lemere, W.K. Cullen, G.M. Shankar, V. Betts, E.T. Spooner, L. Jiang, R. Anwyl, D.J. Selkoe, M.J. Rowan, Amyloid beta protein immunotherapy neutralizes Abeta oligomers that disrupt synaptic plasticity in vivo, Nat Med 11 (2005) 556-561.
[100] D. Puzzo, L. Privitera, E. Leznik, M. Fa, A. Staniszewski, A. Palmeri, O. Arancio, Picomolar amyloid-beta positively modulates synaptic plasticity and memory in hippocampus, J Neurosci 28 (2008) 14537-14545.
[101] J.M. Orgogozo, S. Gilman, J.F. Dartigues, B. Laurent, M. Puel, L.C. Kirby, P. Jouanny, B. Dubois, L. Eisner, S. Flitman, B.F. Michel, M. Boada, A. Frank, C. Hock, Subacute meningoencephalitis in a subset of patients with AD after Abeta42 immunization, Neurology 61 (2003) 46-54.
[102] H. LeVine, 3rd, Q. Ding, J.A. Walker, R.S. Voss, C.E. Augelli-Szafran, Clioquinol and other hydroxyquinoline derivatives inhibit Abeta(1-42) oligomer assembly, Neurosci Lett

465 (2009) 99-103.
[103] H. LeVine, 3rd, L. Lampe, L. Abdelmoti, C.E. Augelli-Szafran, Dihydroxybenzoic acid isomers differentially dissociate soluble biotinyl-Abeta(1-42) oligomers, Biochemistry 51 (2012) 307-315.
[104] H. LeVine, 3rd, Biotin-avidin interaction-based screening assay for Alzheimer's beta-peptide oligomer inhibitors, Anal Biochem 356 (2006) 265-272.
[105] A. Frey, B. Meckelein, D. Externest, M.A. Schmidt, A stable and highly sensitive 3,3',5,5'-tetramethylbenzidine-based substrate reagent for enzyme-linked immunosorbent assays, J Immunol Methods 233 (2000) 47-56.
[106] S. Ruttinger, V. Buschmann, B. Kramer, R. Erdmann, R. Macdonald, F. Koberling, Comparison and accuracy of methods to determine the confocal volume for quantitative fluorescence correlation spectroscopy, J Microsc 232 (2008) 343-352.
[107] A. Michelman-Ribeiro, F. Horkay, R. Nossal, H. Boukari, Probe diffusion in aqueous poly(vinyl alcohol) solutions studied by fluorescence correlation spectroscopy, Biomacromolecules 8 (2007) 1595-1600.
[108] S.T. Hess, S. Huang, A.A. Heikal, W.W. Webb, Biological and chemical applications of fluorescence correlation spectroscopy: a review, Biochemistry 41 (2002) 697-705.
[109] M.A. Medina, P. Schwille, Fluorescence correlation spectroscopy for the detection and study of single molecules in biology, Bioessays 24 (2002) 758-764.
[110] E. Haustein, P. Schwille, Trends in fluorescence imaging and related techniques to unravel biological information, HFSP J 1 (2007) 169-180.
[111] M. Eigen, R. Rigler, Sorting single molecules: application to diagnostics and evolutionary biotechnology, Proc Natl Acad Sci U S A 91 (1994) 5740-5747.
[112] R. Rigler, Fluorescence correlations, single molecule detection and large number screening. Applications in biotechnology, J Biotechnol 41 (1995) 177-186.
[113] U. Meseth, T. Wohland, R. Rigler, H. Vogel, Resolution of fluorescence correlation measurements, Biophys J 76 (1999) 1619-1631.
[114] J.D. Harper, S.S. Wong, C.M. Lieber, P.T. Lansbury, Observation of metastable Abeta amyloid protofibrils by atomic force microscopy, Chem Biol 4 (1997) 119-125.
[115] P.K. Hansma, Cleveland, J. P., Radmacher, M.,, D.A. Walters, Hillner, P. E., Bezanilla, M. et al., Tapping mode atomic-force microscopy in liquids, Appl. Phys. Letters 64 (1994) 1738–1740.
[116] N. Jalili, K. Laxminarayana, A review of atomic force microscopy imaging systems: application to molecular metrology and biological sciences, Mechatronics 14 (2004) 907-945.
[117] H.G. Hansma, K.J. Kim, D.E. Laney, R.A. Garcia, M. Argaman, M.J. Allen, S.M. Parsons, Properties of biomolecules measured from atomic force microscope images: a review, J Struct Biol 119 (1997) 99-108.
[118] P.O. Gendron, F. Avaltroni, K.J. Wilkinson, Diffusion coefficients of several rhodamine derivatives as determined by pulsed field gradient-nuclear magnetic resonance and fluorescence correlation spectroscopy, J Fluoresc 18 (2008) 1093-1101.
[119] S. Nag, B. Sarkar, A. Bandyopadhyay, B. Sahoo, V.K. Sreenivasan, M. Kombrabail, C. Muralidharan, S. Maiti, Nature of the amyloid-beta monomer and the monomer-oligomer equilibrium, J Biol Chem 286 (2011) 13827-13833.

[120] H. Fukumoto, T. Tokuda, T. Kasai, N. Ishigami, H. Hidaka, M. Kondo, D. Allsop, M. Nakagawa, High-molecular-weight beta-amyloid oligomers are elevated in cerebrospinal fluid of Alzheimer patients, FASEB J 24 (2010) 2716-2726.

[121] M.-B.J.A. Carnero-Ruiz C., Aguiar, J, MacIsaac, G., Moroze, S;Palepu, R., EVect of ethylene glycol on the thermodynamic and micellar properties of Tween 20,, Colloid Polym. Sci. 271 (2003) 531–541.

[122] C.J. Pike, D. Burdick, A.J. Walencewicz, C.G. Glabe, C.W. Cotman, Neurodegeneration induced by beta-amyloid peptides in vitro: the role of peptide assembly state, J Neurosci 13 (1993) 1676-1687.

[123] A.E. Roher, M.O. Chaney, Y.M. Kuo, S.D. Webster, W.B. Stine, L.J. Haverkamp, A.S. Woods, R.J. Cotter, J.M. Tuohy, G.A. Krafft, B.S. Bonnell, M.R. Emmerling, Morphology and toxicity of Abeta-(1-42) dimer derived from neuritic and vascular amyloid deposits of Alzheimer's disease, J Biol Chem 271 (1996) 20631-20635.

[124] P. Sengupta, K. Garai, J. Balaji, N. Periasamy, S. Maiti, Measuring size distribution in highly heterogeneous systems with fluorescence correlation spectroscopy, Biophys J 84 (2003) 1977-1984.

[125] J. Skilling, Bryan, R. K. , Maximum entropy image reconstruction: general algorithm, Mon. Not. R. Astr. Soc. 211 (1984) 111–124.

[126] B. Sahoo, S. Nag, P. Sengupta, S. Maiti, On the stability of the soluble amyloid aggregates, Biophys J 97 (2009) 1454-1460.

VITA

CHEN CHEN

Personal:
Place of Birth: Yangzhou, Jiangsu, China

Education:
2010-2011: Master of Science, Analytical Chemistry, Hong Kong Baptist University
2006-2010: Bachelor of Engineering, Bioengineering, Yangzhou University

Professional positions:
2012-2013: Teaching Assistant, Department of Chemistry, University of Kentucky

Publication:
X. Chen, J. Yin, N. Zhang, C. Chen, S. Yang, X. Jiao, Prevalence and transmission of plasmid-mediated quinolone resistance *qnrS* gene among *Escherichia coli* isolates in a poultry farm, Acta Microbiologica Sinica 10 (2013).